

12-31-2019

Impact of stirrer speed and media type-loading on the breakage kinetics during wet stirred media milling of griseofulvin

Nathaniel Parker
New Jersey Institute of Technology

Follow this and additional works at: <https://digitalcommons.njit.edu/theses>



Part of the [Chemical Engineering Commons](#)

Recommended Citation

Parker, Nathaniel, "Impact of stirrer speed and media type-loading on the breakage kinetics during wet stirred media milling of griseofulvin" (2019). *Theses*. 1744.
<https://digitalcommons.njit.edu/theses/1744>

This Thesis is brought to you for free and open access by the Electronic Theses and Dissertations at Digital Commons @ NJIT. It has been accepted for inclusion in Theses by an authorized administrator of Digital Commons @ NJIT. For more information, please contact digitalcommons@njit.edu.

Copyright Warning & Restrictions

The copyright law of the United States (Title 17, United States Code) governs the making of photocopies or other reproductions of copyrighted material.

Under certain conditions specified in the law, libraries and archives are authorized to furnish a photocopy or other reproduction. One of these specified conditions is that the photocopy or reproduction is not to be “used for any purpose other than private study, scholarship, or research.” If a user makes a request for, or later uses, a photocopy or reproduction for purposes in excess of “fair use” that user may be liable for copyright infringement,

This institution reserves the right to refuse to accept a copying order if, in its judgment, fulfillment of the order would involve violation of copyright law.

Please Note: The author retains the copyright while the New Jersey Institute of Technology reserves the right to distribute this thesis or dissertation

Printing note: If you do not wish to print this page, then select “Pages from: first page # to: last page #” on the print dialog screen

The Van Houten library has removed some of the personal information and all signatures from the approval page and biographical sketches of theses and dissertations in order to protect the identity of NJIT graduates and faculty.

ABSTRACT

IMPACT OF STIRRER SPEED AND MEDIA TYPE-LOADING ON THE BREAKAGE KINETICS DURING WET STIRRED MEDIA MILLING OF GRISEOFULVIN

**by
Nathaniel Parker**

The aim of this study is to investigate the impact of stirrer speed (2000–4000 rpm) and bead loading (~20–60%) on the breakage kinetics–energy consumption during milling of griseofulvin, a poorly soluble drug, and compare the performance of crosslinked polystyrene (CPS) beads with that of yttrium-stabilized zirconia (YSZ) beads. Laser diffraction, SEM, viscometry, and XRPD were used for characterization. A microhydrodynamic model was used to interpret the breakage kinetics. An increase in stirrer speed led to faster breakage due to more frequent and forceful CPS bead–bead collisions. Despite causing slight decrease in maximum contact pressure, an increase in CPS bead loading caused a dramatic increase in frequency of drug particle compressions, which dominated the faster breakage. While YSZ beads required higher energy consumption than CPS beads, they achieved the same product fineness faster than CPS beads. Microhydrodynamic model rationalized the favorable use of YSZ over CPS beads.

**IMPACT OF STIRRER SPEED AND MEDIA TYPE-LOADING ON THE
BREAKAGE KINETICS DURING WET STIRRED MEDIA MILLING OF
GRISEOFULVIN**

**by
Nathaniel Parker**

**A Thesis
Submitted to the Faculty of
New Jersey Institute of Technology
in Partial Fulfillment of the Requirements for the Degree of
Master of Science in Chemical Engineering**

**Otto H. York Department of
Chemical and Materials Engineering**

December 2019

Blank Page

APPROVAL PAGE

**IMPACT OF STIRRER SPEED AND MEDIA TYPE-LOADING ON THE
BREAKAGE KINETICS DURING WET STIRRED MEDIA MILLING OF
GRISEOFULVIN**

Nathaniel Parker

Dr. Ecevit A. Bilgili, Thesis Advisor
Associate Professor of Chemical and Materials Engineering, NJIT

Date

Dr. Piero M. Armenante, Committee Member
Distinguished Professor of Chemical and Materials Engineering, NJIT

Date

Dr. Murat Guvendiren, Committee Member
Assistant Professor of Chemical and Materials Engineering, NJIT

Date

BIOGRAPHICAL SKETCH

Author: Nathaniel David Parker

Degree: Master of Science

Date: January 2020

Undergraduate and Graduate Education:

- Master of Science in Chemical Engineering,
New Jersey Institute of Technology, Newark, NJ, 2020
- Bachelor of Science in Chemical Engineering,
New Jersey Institute of Technology, Newark, NJ, 2018

Major: Chemical Engineering

The thesis work was dedicated to my beloved family. My sisters Amanda and Rachel, my nephew Judah, and my soon to be nephew David. And in remembrance of my parents,
David and Joan Parker.

ACKNOWLEDGMENT

I would like to express my deepest appreciation to my thesis advisor, Dr. Ecevit Bilgili, whose drive for knowledge would motivate and inspire me, and dedication to his students guided me through out my research. I would like to thank Dr. Piero Armenante and Dr. Murat Guvendiren for serving as my committee members.

I also want to thank Dr. Mahbubur Rahman who was my mentor and helped me learn a lot from scratch. I would also like to thank Eylül, Gülizar, Nontawat, and Zhixing for helping me and keeping me focused in the right direction.

TABLE OF CONTENTS

Chapter	Page
1 INTRODUCTION.....	1
1.1 Background Information.....	1
1.1.1 Wet Stirred Media Milling	1
1.1.2 Impact of Wet Stirred Media Milling Parameters.....	4
1.1.3 Physical Stability of the Milled Suspensions.....	6
1.1.4 Approaches in Modeling for Wet Media Milling	7
1.2 Issues and Knowledge Gap.....	13
1.3 Scope and Organization of Thesis.....	17
2 EXPERIMENTAL.....	18
2.1 Preparation of Griseofulvin Nanosuspensions.....	18
2.2 Characterization Techniques.....	22
3 THEORETICAL.....	25
3.1 Analysis of Breakage Kinetics.....	25
3.2 Microhydrodynamic Analysis.....	26
4 RESULTS AND DISCUSSION.....	30
4.1 Effects of Wet Media Milling on Griseofulvin Particle Size and Morphology.....	30
4.2 Impact of Process Parameters on Breakage Kinetics–Energy Consumption for Cross–linked Polystyrene Beads.....	34
4.2.1 Impact of Stirrer Speed and Bead Loading.....	35

TABLE OF CONTENTS
(Continued)

Chapter	Page
4.2.2 Microhydrodynamic Analysis of the Impact of Process Parameters for Cross-linked Polystyrene Beads.....	45
4.3 Impact of Media Material: A Comparative Analysis.....	49
4.3.1 Impact of Media Material on Breakage Kinetics	50
4.3.2 Microhydrodynamic Analysis of the Impact of Media Material in Wet Stirred Media Milling.....	53
4.4 An Engineering Rationale for the Selection of Bead Material.....	55
5 CONCLUSIONS AND OUTLOOK.....	58
APPENDIX A.....	60
APPENDIX B.....	62
APPENDIX C.....	69
REFERENCES.....	72

LIST OF TABLES

Table	Page
1.1 Brief Overview of Pharmaceutical Literature using Polystyrene Media in Nanoparticle Production.....	15
2.1 Process parameters and Bead Material Investigated in Milling Experiments.....	21
3.1 Particle Size Statistics of the Suspensions after 256 min of Milling and 7-day Storage.....	31
B.1 The Time it Takes for the Drug Median Size d_{50} to Reach $0.5\ \mu\text{m}$ (t_{d50}) and d_{90} to Reach $1\ \mu\text{m}$ (t_{d90}) and Characteristic Time Constant (τ_p) Fitted by the Empirical Model (Eq. (4.1)) to the Evolution of the Median Particle Size.	62
B.2 Values for Characteristic Milling Times (t_{d50} and t_{d90}), Energy Consumption for t_{d50} (E_{td50}), Energy Consumption for t_{d90} (E_{td90}), and Merit Scores for Run 2–15.....	63
B.3 Power Applied Per Unit Volume P_w , Apparent Shear Viscosity μ_L and Density ρ_L of the Milled Drug Suspensions Measured, and Dynamic Viscosity μ_m and Mixture Density ρ_m of the Slurries Estimated for Runs 1–15.....	64
B.4 Power applied per unit volume P_w and all microhydrodynamic parameters (θ , u_b , v , σ_b^{\max} , α_b , a , and $\Pi \cdot \sigma_y$) calculated for Runs 1–15.....	65

LIST OF FIGURES

Figure		Page
1.1	Schematic of a Netzsch stirred media mill operating in the recirculation mode. P and T represent pressure transducer and thermocouple, respectively.....	3
2.1	Image of the Netsch (Microcer) wet stirred media mill in recirculatory mode.....	20
2.2	Images of the milling chamber (a) empty, (b) with CPS beads at a bead loading of $c = 0.198$ and (c) a bead loading of $c = 0.594$	22
4.1	SEM images of (a) as-received GF particles and GF particles after 256 min of milling with (b) $\omega = 2000$ rpm with $c = 0.198$ using CPS beads (Run 1), (c) $\omega = 4000$ rpm with $c = 0.594$ using CPS beads (Run 12), and (d) $\omega = 4000$ rpm with $c = 0.594$ using YSZ beads (Run 15). Scale bar indicates 2 μm in (a), 1 μm in (b), and 100 nm in (c) and (d).....	32
4.2	XRPD diffractograms of (a) as-received GF, HPC, and SDS, and (b) unmilled physical mixture of GF–HPC–SDS, and dried, milled suspensions of Runs 1 and 12. Run 1 refers to the drug suspension milled at $\omega = 2000$ rpm with $c = 0.198$ and Run 12 refers to the drug suspension milled at $\omega = 4000$ rpm with $c = 0.594$	33
4.3	Effects of CPS bead loading c on the time-wise evolution of d_{50} and d_{90} during wet stirred media milling of GF particles at various stirrer speeds: (a) $\omega = 2000$ rpm, (b) $\omega = 3000$ rpm, and (c) $\omega = 4000$ rpm. At $t = 0$, the GF particles had $d_{50} = 13.73 \pm 0.087$ μm and $d_{90} = 33.96 \pm 0.711$ μm	37
4.4	Effects of CPS bead loading c on characteristic milling times t_{d50} , t_{d90} , and τ_p at various stirrer speeds: (a) $\omega = 2000$ rpm, (b) $\omega = 3000$ rpm, and (c) $\omega = 4000$ rpm. Note, for $\omega = 2000$ rpm and $c = 0.198$, d_{50} and d_{90} did not reach 0.5 μm and 1 μm , respectively.....	38
4.5	Effects of stirrer speed ω and CPS bead loading c on the average power consumption per unit volume P_w for Runs 1–12.....	41
4.6	Effects of stirrer speed ω and CPS bead loading c on the specific energy consumption during t_{d50} (E_{td50}) for Runs 2–12.....	42
4.7	Effects of stirrer speed ω and CPS bead loading c on specific energy consumption during t_{d90} (E_{td90}) for Runs 2–12.....	43

**LIST OF FIGURES
(Continued)**

Figure	Page
4.8 Effects of stirrer speed ω and CPS bead loading c on the Merit score (-) for Runs 2–12.....	44
4.9 Effects of CPS bead loading c on granular temperature θ , average bead oscillation velocity u_b , and frequency of single-bead oscillation ν at various stirrer speeds: (a) $\omega = 2000$ rpm, (b) $\omega = 3000$ rpm, and (c) $\omega = 4000$ rpm (Runs 1–12).....	47
4.10 Effects of CPS bead loading c on the maximum contact pressure σ_b^{\max} , the average frequency of drug particle compressions a , and the pseudo energy dissipation rate $\Pi \cdot \sigma_y$ at various stirrer speeds: (a) $\omega = 2000$ rpm, (b) $\omega = 3000$ rpm, and (c) $\omega = 4000$ rpm (Runs 1–12).....	48
4.11 Optical microscope image of 400 μm nominal sized (a) CPS beads (measured median size: 444 μm) and (b) YSZ beads (measured median size: 405 μm) and (c) particle size distributions of the beads.....	49
4.12 Effects of bead material, i.e., CPS vs. YSZ, on the evolution of the median size of GF particles beads at a fixed bead loading of $c = 0.594$ and various stirrer speeds: (a) $\omega = 2000$ rpm, (b) $\omega = 3000$ rpm, and (c) $\omega = 4000$ rpm. At $t = 0$, the GF particles had $d_{50} = 13.73 \pm 0.087$ μm and $d_{90} = 33.96 \pm 0.711$ μm	51
4.13 Effects of stirrer speed on the characteristic milling times, energy consumptions, and merit score: (a) t_{d50} and E_{td50} (b) t_{d90} and E_{td90} , and (c) τ_p and merit score when CPS and YSZ beads were used. Lines illustrate characteristic times; bars illustrate energy consumptions and merit score.	52
4.14 Effects of stirrer speed on (a) granular temperature θ , (b) the average bead oscillation velocity u_b , (c) the average frequency of drug particle compressions a , (d) the maximum contact pressure σ_b^{\max} , (e) radius of the contact circle α_b , and (f) the pseudo energy dissipation rate $\Pi \cdot \sigma_y$ when CPS and YSZ beads were used.....	54
B.1 Apparent shear viscosity of the milled suspensions prepared in Runs 1–15 at various stirrer speeds: (a) $\omega = 2000$ rpm, (b) $\omega = 3000$ rpm, and (c) $\omega = 4000$ rpm, along with that of the aqueous stock solution of the stabilizers (5% HPC SL grade and 0.5% SDS), shown for baseline comparison. The stock solution was not processed in the mill.....	68

CHAPTER 1

INTRODUCTION

1.1 Background Information

Several new drugs in the developmental stages exhibit a common trait of having poor water solubility and therefore have low bioavailability (Merisko-Liversidge and Liversidge, 2011). One method of overcoming this challenge is by increasing the surface area of the drug by creating nanoparticles. An increase in surface area can improve dissolution rates (Noyes and Whitney, 1897) and therefore the bioavailability of the drug. By decreasing the drug particles down to the nanoscale, especially those with sizes less than 100 μm , show higher saturation solubility which enhances the dissolution rate. There are several methods to creating drug nanoparticles, these methods generally fall into two categories Top-down and bottom-up, where in a top-down approach bulk material is broken down to finer particles where as in the bottom-up approach nanoparticles are synthesized. Some examples of these two approaches include, bottom up: antisolvent precipitation (Kakran et al. 2012, Yadav and Kumar et al. 2014), melt emulsification (Bhakay et al. 2016) etc. and top-down: high-pressure homogenization (Silva et al. 2011, Sun et al. 2011), wet media milling (Bitterlich et al. 2015, Toziopoulou et al. 2017, Ye et al. 2014).

1.1.1 Wet Media Milling

Among the top-down methods previously mentioned, wet media milling is one of the most common unit operations in the pharmaceutical industry. Wet media milling is a robust and solvent free method in preparing drug nanoparticles. In this technique a pre-suspension is

prepared by mixing micronized drug particles with a solution of stabilizers consisting of polymers and/or surfactants. The pre-suspension is then milled with a grinding media (beads). Drug particles are captured between the colliding beads inducing stresses on the particles causing them to fatigue and break. Prolonged exposure to these stresses eventually brings the drug particles down to nano scale in which the accepted term of nanoparticles is particles of sizes below to 1 μm (Peltonen and Hirvonen, 2010). Wet media milling holds distinct advantages over other methods such as: relatively high drug loading, minimal excipient side effects, the ability of continuous operation, and can be implemented in the size reduction of most poorly water-soluble drug candidates (Müller et al. 2001). Several marketed products that have implemented wet media milling in their processing include: Rapamune[®] (Pfizer (Wyeth), New York City, NY, USA), Emend[®] (Merck, Kenilworth, NJ, USA), Invega[®] Sustenna[®] Xeplion[®] (Janssen, Beerse, Belgium) and Tricor[®] Lipanthyl[®] (Abbott Laboratories, Fournier Pharma, Montréal, QC, Canada).

There are various types of wet media milling equipment such as planetary mills (Liu et al. 2011), acoustic mixing (Leung et al. 2014), orbital shaker (Van Eerdenbrugh et al. 2009) but wet stirred media mills (WSMM) are among the most widely used and most relevant to industrial processes (Ghosh et al. 2012). When the final particle sizes are reached, the nanosuspension can be implemented in several delivery methods such as: oral, injectable, and nebulized inhalation (Cooper 2010). However, a common method is drying the nanosuspension into powders for standard dosage forms such as capsules and tablets (Van Eerdenbrugh et al. 2008) When WSMM is used in recirculation mode, suspension circulates initially from a holding tank to the milling chamber. Immediately exiting the milling chamber is a screen with opening that is usually half the nominal size of the milling

beads. The screen ensures the beads are retained in the milling chamber and are not circulated with the suspension. After passing the screen the suspension is returned to the holding tank, where the cycle repeats itself. Figure 1.1 is a schematic representation of a recirculating wet stirred media mill.

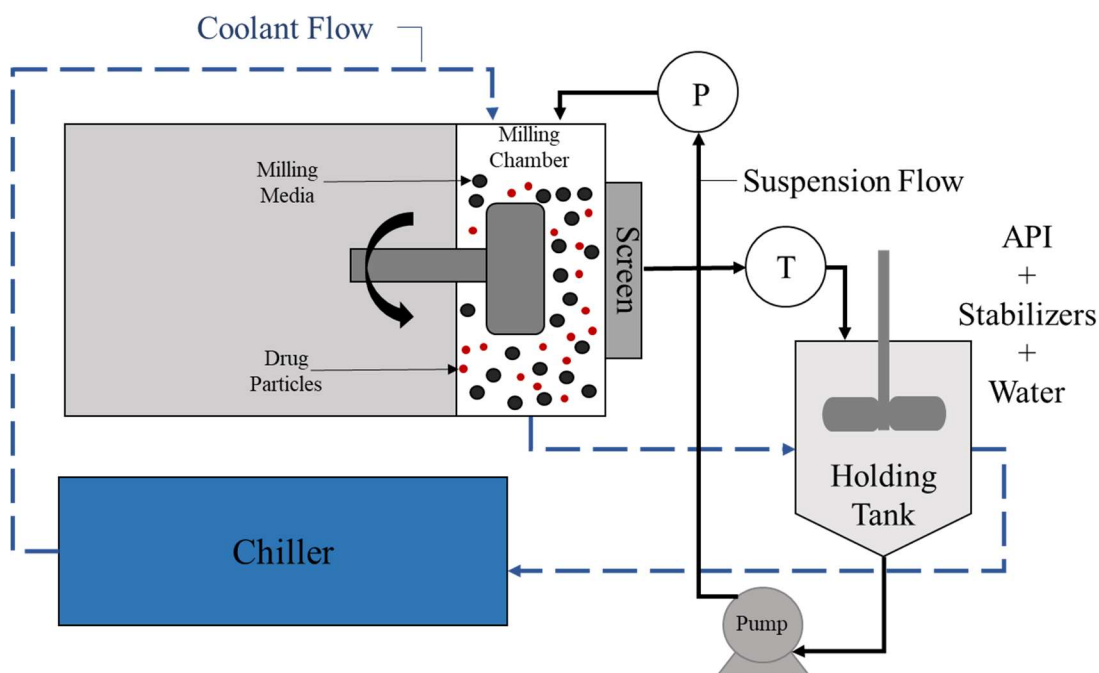


Figure 1.1 Schematic of a Netzsch stirred media mill operating in the recirculation mode. P and T represent pressure transducer and thermocouple, respectively.

Wet media milling has proven to be a robust approach in producing nanosuspensions of a variety of poorly water-soluble drugs. However, challenges arise in the process as it is time-consuming, costly, and energy intensive (Kawatra 2006). These issues are recognized by the pharmaceutical industry yet most literature focuses on stabilization of the suspension itself. While ensuring a stable suspension is critical in creating nanosuspensions, having an understanding of the effect process parameters can mitigate some of the aforementioned issues. Since the breakage kinetics during milling can

dictate the fineness of the final product and therefore cycle time, it is fundamentally important to understand the effect of processing conditions on the breakage kinetics.

1.1.2 Impact of Wet Stirred Media Milling Parameters

Varying process parameters such as bead loading, stirrer speed, drug loading, milling time, and suspension flow rate can have substantial effects on the breakage kinetics and the time required for the milling process (Afolabi et al., 2014). Stirrer speed is an important process parameter, as increasing stirrer speed leads to higher bead velocities and oscillations (Afolabi et al. 2014). Stirrer speeds with circumferential speeds ranging from 150–6000 rpm and tip speeds of 6.9–16.4 m/s have been reported in literature (Date and Patravale 2004, Kwade 1999, Nakach et al. 2018). It has been observed in previous studies (Li et al. 2015, Singh et al. 2011, Tanaka et al. 2012) that increasing stirrer speed led to smaller particle sizes at any given point in time. Implying, that increasing stirrer speed results in a faster apparent breakage rate.

Bead loading, in general, is the ratio of the true volume of the beads to volume of the milling chamber. Afolabi et al. 2014 found that an increase in bead loading led to a faster breakage rate and smaller final particle size of griseofulvin. Similar observations were made by Li et al. and Patel et al. 2010. Patel et al. 2010 suggested the results are due to smaller voids between the beads which prevented aggregation of the drug during milling. However, Afolabi et al. 2014 and Li et al. 2015 conducted their experiments using a properly stabilized suspension, ruling out the prevention of aggregation as the reason. Both Afolabi et al. 2014 and Li et al. 2015 applied a microhydrodynamic model to their results and found that the increase in bead loading led an increase in the number of bead–bead collisions. However, as bead loading increased, a decrease in the stresses applied by the

beads were observed. This suggests there are two competing effects when increasing bead loading: lower stressful events occur and the number of stressful events increase.

Afolabi et al. 2014 varied drug loading from 5% to 30 % w/v and found that an increase in drug loading led to a slower breakage rate. Similar results were found in other studies (Ghosh et al. 2012, Nakach et al. 2017). Nakach et al. 2017 varied drug loading from 5% to 40% and found as drug loading increased an increase in milling time was needed to reach a similar final particle size and suggested that an increase in drug loading led to an increase in viscosity which then resulted in slower breakage. Despite the slower breakage rate, an increase in drug loading results in a higher amount of drug being processed per batch. Afolabi et al. 2014 found that as drug loading increased specific energy consumption decreased. Considering the time needed in preparation/cleaning for each batch, higher drug loading can be operationally more efficient.

The duration of milling time, even in small scale operation, can vary greatly from 30 min (Bhakay et al. 2011) to a day (Bitterlich et al. 2014). However, this is relative to the milling design, batch size, and specific energy. Regardless of the milling equipment, milling for longer periods of time generally leads to a decrease in particle size (Deng et al. 2008, Ghosh et al. 2012, Singh et al. 2011). Increasing the milling time allows for more drug particle compressions and bead-bead collisions which reduces the overall amount of unmilled particles in the suspension. While prolonging milling shows a decrease in particle size, it is well known that a grinding limit or dynamic equilibrium particle size is reached and particle sizes begin to plateau (Knieke et al. 2013). This suggests that prolonged milling time for desired drug particle size can lead to a higher energy expenditure which could also result in contamination from bead wear.

1.1.3 Physical Stability of the Milled Suspensions

A fundamental challenge in WSMM and the creation of nanoparticles is the physical stability of the suspension. Physical stability of a suspension is generally defined as having a minimal amount of aggregates in the suspension and a negligible size increase of the particles after the milling process. During the milling process particles are broken down, and as a result an increase in surface area is observed. Because of the increase in surface area, nanosuspensions are thermodynamically unstable (Malamatari et al. 2018) and therefore have a tendency to aggregate. Two major competing mechanisms occur during WSMM: particles being broken down from the stresses created by the beads and attractive inter-particle forces causing particles to aggregate (Bhakay et al. 2013, Cerdeira et al. 2010)

When dispersed in a liquid medium, drug particles are stabilized by either a steric or electrostatic mechanism or a combination of both (electrosteric mechanism) which is achieved by the polymers and/or surfactants (Peltonen and Hirvonen 2010, Van Eerdenbruggen et al. 2008). Nonionic polymers and surfactants create steric stabilization by adsorbing on to the drug surface and preventing particles from entering a proximity where van der Waals forces can cause aggregation. Some common types of steric stabilizers are cellulose derivatives, poloxamers, polysorbates, and providones.

While some surfactants can act as steric stabilizers, ionic surfactants create electrostatic stabilization by providing repulsion of particles with similar charge. Surfactants also reduce the surface tension between drug particles and the liquid medium. This in turn promotes the wetting of the drugs surface. Electrosteric stabilization occurs when nonionic polymers and ionic/nonionic surfactants act on the drug particles simultaneously. The use of both polymers and surfactants together have been shown to

create synergistic effects in stabilizing suspensions (Basa et al. 2008, Bilgili et al. 2016, Nakach et al. 2014). Nakach et al. (2014) used the polymer polyvinylpyrrolidone (PVP) and sodium dodecyl sulfate (SDS) as stabilizers. They found that while PVP alone and the combination of PVP and SDS produced similar final particle sizes, the use of PVP alone exhibited severe aggregation over the next 7 and 14 days. However, other studies (Monteiro et al. 2013) have shown that this synergistic effect not only promotes physical stability of the milled suspensions but also helps in the particle breakage during milling.

1.1.4 Approaches in Modeling for Wet Media Milling

While evaluating the breakage kinetics reveals insight as to the effects of varying process parameters, it does not give a fundamental understanding or quantitative reasoning as to why the results are occurring. WSMM has shown to be a robust method of creating nanoparticles for the enhancement of poorly water-soluble drugs, however it is also energy intensive and costly. Therefore, it would be beneficial to quantify the results observed through a mathematical model in order to optimize the breakage kinetics. However, only a few studies (Afolabi et al. 2014, Annapragada and Adjei 1996, Bilgili and Afolabi 2012, Li et al. 2015) have been reported that applied a model in drug nanomilling.

During WSMM, energy consumption is an important quantity as this energy is transferred to the beads and suspension which promotes breakage of the particles. However, only a part of the energy consumed during milling is imparted to the beads (Kwade 1999, Li et al. 2016). It has been suggested that the energy used in causing breakage is substantially smaller than the energy associated with viscous dissipation (Eskin et al. 2005). Cerdeira et al. (2011) evaluated the specific energy input to particle sizes during milling. This was done while varying process parameters such as: bead size, bead

loading, product flow rate, and stirrer speed. They showed as particle size decreased the specific energy input increased, which is intuitive as some of the energy consumed in the milling process is used in particle breakage. These results are similar to Afolabi et al. (2014) who found that as stirrer speed and bead concentration increased the specific energy increased and faster particle breakage was observed. Koonerth et al. (2016) showed a correlation between the specific energy, particle size, and bead size. They found that larger bead sizes not only produced larger particles but also larger specific energy consumptions. Li et al. (2017) found similar results but conducted the experiments more systematically by also varying stirrer speed and applying a microhydrodynamic model.

It has been observed from experimental data when milling various materials (Stražičar and Runovc 1996, Varinot et al. 1999), the particle size evolution follows a first order exponential decay in time t . Experimental data (Afolabi et al. 2014, Bilgili and Afolabi 2012) was fitted to the following empirical model:

$$d_{50}(t) = d_{\text{lim}} + [d_{50}(0) - d_{\text{lim}}] \exp(-t / \tau_p) \quad (1.1)$$

where $d_{50}(0)$ is the initial median particles size at $t = 0$, d_{lim} is the limiting particle size given enough milling time, and τ_p is a characteristic time constant associated with the milling kinetics, where a lower τ_p value corresponds to faster breakage kinetics. Using this empirical model and analyzing τ_p , the effect of process parameters on breakage kinetics was evaluated. Experimental data was fitted using SigmaPlot's non-linear regression wizard that uses a Marquardt-Levenberg algorithm to minimize the sum of squared residuals, given by the following:

$$SSR = \sum_{i=1}^n \left[\log_{10}(d_{50i}^{\text{exp}}) - \log_{10}(d_{50i}^{\text{mod}}) \right]^2 \quad (1.2)$$

where the superscripts are denoted as the “exp” for the experimental data and “mod” as values from model in Equation (1). These values are indexed by different time points i , where i is some integer ($i = 1, 2 \dots n$). Because aggregation can become problematic when wanting to solely examine the breakage kinetics, a polymer-surfactant combination to create a well stabilized suspension should be used.

While examining the specific energy consumption on particle breakage and using descriptive dynamic models can reveal insight on the breakage kinetics, neither give information on bead dynamics during WSMM. Until recently, the microhydrodynamics, which is considered the fluctuating motion of beads in a sheared suspension, has not been studied in literature. By use of the kinetic theory of granular flows and fundamental energy balances (Gidaspow, 1994), Eskin et al. (2005a,b) developed a microhydrodynamic model which reveals information on the turbulent nature of the beads during the milling process. From the model, it is assumed the power applied to the stirrer is evenly distributed to the entire volume of the slurry (beads and suspension) and can be expressed as the total energy dissipation rate ε_{tot} . While taking into account the fluctuating motion of the beads and liquid-bead viscous friction at the micro-scale, the total power dissipation rate is expressed as:

$$P_w = \varepsilon_{\text{tot}} = \varepsilon_{\text{visc}} + \varepsilon_{\text{coll}} \quad (1.3)$$

where P_w is the power applied to the stirrer per unit volume, $\varepsilon_{\text{visc}}$ is the energy dissipation rate due to liquid-bead viscous friction and lubrication, and $\varepsilon_{\text{coll}}$ is the energy dissipation

rate due to partially inelastic bead collisions. However, these terms do not capture the energy dissipation due to the friction losses between liquid layers. Motivated by the work of Eskin and Miller (2008) on slurry flow in fractures, a new term was introduced by Bilgili and Afolabi (2012) as ε_{ht} . ε_{ht} is defined as the power attributed to shearing the equivalent liquid (milled suspension) as if no beads were present, the modified equation is now expressed as:

$$P_w = \varepsilon_{tot} = \varepsilon_{visc} + \varepsilon_{coll} + \varepsilon_{ht} \quad (1.4)$$

Following from Eskin et al. (2005a,b) the total power applied to the stirrer per unit volume can be represented as:

$$P_w = \frac{54\mu_L c \theta R_{diss}}{d_b^2} + \frac{12}{d_b \sqrt{\pi}} (1 - k^2) \left[\frac{1 - 0.5c}{(1 - c)^3} \right] c^2 \rho_b \theta^{3/2} + \varepsilon_{ht} \quad (1.5)$$

where μ_L is the apparent shear viscosity, c is the volumetric bead concentration (bead loading), θ is the granular temperature (bead-equivalent liquid relative root-mean velocity), R_{diss} is the effective drag coefficient, d_b is the median size of the milling bead, k is the coefficient of restitution during bead-bead collisions, and ρ_b is the bead density. Power applied to the stirrer per unit volume P_w , the energy dissipation rate of shearing the equivalent liquid ε_{ht} , and apparent shear viscosity μ_L were measured. Accompanied with bead properties, the measured values can be incorporated into Equation (5) and the granular temperature can be solved using a non-linear equation solver. Knowing the granular temperature θ the energy dissipation rate attributed to the deformation of the drug particles per unit volume Π can be determined:

$$\Pi = 2.23 \frac{c^2(2-c)}{(1-c)^3 \pi^{5/2} \varepsilon \sigma_y} \left[\frac{Y_b}{1-\eta_b^2} \right]^{18/15} \left(\frac{Y^*}{Y_p} \right)^\gamma \rho_b^{4/5} \frac{R_p}{(R_b)^2} \theta^{13/10} \quad (1.6)$$

here, ε , σ_y , Y_b , η_b , Y^* , R_b , and R_p are the volume fraction of the drug in the suspension, contact pressure in the drug particle when fully plastic condition is reached, the Young's modulus of the beads, the Poisson ratio of the beads, reduced elastic modulus of the bead-particle contact, radius of the bead, and radius of the drug particles, respectively. However, to be able to calculate Π , mechanical properties of the drug particles must be known or measured. Since it is difficult to measure these values and find reliable values in literature, Afolabi et al. (2014) decomposed Π into two parts: a material dependent factor λ and a process-dependent factor F , and are expressed as:

$$\lambda = 2.23 \frac{1}{\pi^{5/2} \sigma_y} \left(\frac{Y_b}{1-\eta^2} \right)^{18/15} \left(\frac{Y^*}{Y_p} \right)^\gamma \rho_b^{4/5} \frac{R_p}{R_b^2} \quad (1.7)$$

$$F = \frac{c^2(2-c)}{(1-c)^3 \varepsilon} \theta^{13/10} \quad (1.8)$$

With changing process parameters an increase/decrease in F corresponds to a proportional increase/decrease in Π given, sizes of the specific drug-bead materials λ can be considered constant. Other microhydrodynamic parameters such as average bead oscillation velocity u_b , frequency of a single bead oscillation ν , maximum contact pressure during bead-bead collision σ_b^{\max} , and average frequency of drug particle compressions a

can also be calculated. For more detailed information on the microhydrodynamic model, refer to the theoretical section (CHAPTER 3).

Bilgili and Afolabi (2012), Afolabi et al. (2014), and Li et al. (2017) used the microhydrodynamic model to elucidate the impact of process parameters during WSMM and found the following insights:

- Bilgili and Afolabi (2012) found an optimal concentration of HPC when milling griseofulvin during WSMM. This was explained through a combined microhydrodynamic-adsorption analysis, in which an increase in HPC concentration led to a lower θ value due to viscous dampening but an increase in HPC adsorption onto drug particles.
- Afolabi et al. (2014) and Li et al. (2017) found that an increase in stirrer speed led to an all microhydrodynamic parameters increased monotonically. In other words, more mechanical energy was imparted to the slurry resulting in more energetic bead–bead collisions and a higher frequency of drug particles compressions.
- Afolabi et al. (2014) observed that varying bead loading led to two counter acting effects: while v and a increased with increasing bead loading, θ , u_b , and σ_b^{\max} decreased. In other words, while increasing bead loading increases the drug particle compressions, less energetic compressions occur. This led to faster breakage and was explained through an increase in the milling intensity factor F .
- Microhydrodynamic parameters decreased moderately when drug loading was increased, except the milling intensity factor F (Afolabi et al. 2014) which showed a more drastic decrease, explaining the slower breakage rate observed.
- When varying bead diameters d_b Li et al. 2017 found similar results to Afolabi et al. (2014) when varying c : as bead size decreased, θ , u_b , and σ_b^{\max} decreased while v and a increased. However, F could not explain the observed breakage rate alone when varying bead size.

1.2 Issues and Knowledge Gap

A great majority of WSMM studies have used yttrium-stabilized zirconia (YSZ) beads as milling media (Koradia et al., 2018; Ito et al. 2016) as YSZ beads are wear-resistant and have been proven to effectively break drug particles. A commonly held notion is that their high density allows for generation of high stresses during wet media milling, which can induce fast breakage during milling (Nakach et al., 2018). Apart from zirconia beads, crosslinked polystyrene (CPS) beads have been used and they are wear-resistant like YSZ beads. Since CPS beads are lighter and softer than YSZ beads, their media performance in WSMM in terms of breakage kinetics, final milled particle size, and energy consumption are expected to be quite different. Table 1.1 presents an overview of the WSMM studies with CPS beads in the last two decades. A cursory look at these studies reveals that most studies did not examine breakage kinetics—energy consumption and impact of process parameters in a thorough and systematic manner. Interestingly, most studies did not even report bead loading. This is not surprising as these studies such as Onoue et al. (2009) and Quinn et al. (2012) focused on the impact of drug nanoparticles in animal studies and preparing stable drug nanosuspensions. Other studies (Bhakay et al., 2011; Thombre et al., 2012) compared final milled particle sizes of drugs using different types of milling equipment such as jet mill and attritor mill. Some studies (Dai et al., 2007, Deng et al., 2008, Fakes et al., 2009) have investigated the impact of process parameters such as milling time and stirrer speed but did not examine breakage kinetics or energy consumption. Only a few studies (Nakach et al., 2017, Nakach et al., 2018) have investigated the impact of process parameters on the breakage kinetics. However, they treated the wet media milling process as a “black box”, and their findings were purely empirical.

Both polystyrene and zirconia beads have been used in the same experimental studies (Forrest et al., 2018; Juhnke et al., 2010; Nakach et al., 2014), but with different milling equipment/process, which renders a head-to-head comparison impossible. For instance, Leung et al. (2014) used CPS beads in a stirred media mill and YSZ beads in acoustic vibratory mill. Rundfeldt et al. (2013) used both beads in a stirred media mill; but, they only compared the impact of the contamination of the materials, without examining the breakage kinetics of the drug. Kim et al. (2011) also used both beads in a stirred media mill, but only performed one experiment using CPS beads and reported final particle sizes without revealing any information on breakage kinetics. Nakach et al. (2018) analyzed the breakage kinetics using both materials in a stirred media mill, but only compared one experiment using each material and made no systematic comparison. In this study it was found that YSZ beads showed faster breakage than CPS beads. Most importantly, all previous studies provided empirical understanding of the impact of these bead materials. While there have been attempts at investigating the comparative performance of the two bead materials, a head-to-head, fair, scientific examination of CPS beads and YSZ beads in terms of their impact on both the breakage kinetics and the specific energy consumption, does not exist in literature. Considering the energy-intensive, costly, and slow nature of the WSMM, a study of these aspects in a systematic, holistic manner is warranted.

Table 1.1 Process Parameters in Wet Media Milling Studies with Polystyrene Beads used for Preparation of Drug Nanosuspensions.

Stirrer Speed (rpm)	Bead Size (μm)	Bead Loading	Kinetics and Energy Consumption Studied	Microhydrodynamics Studied	References (Year)
6.9–16.4 ^a , 7.0–17.4 ^a	500	0.22–0.90 ^b	Yes	No	Nakach et al. (2018)
(-) ^b	500	(-) ^c	No	No	Forrest et al. (2018)
4000	500	2.17 g	No	No	Leung et al. (2014)
(-) ^b	(-) ^b	(-) ^c	Yes	No	Rundfeldt et al. (2013)
2100	500	(-) ^c	No	No	Thombre et al. (2012)
5000	500	(-) ^c	No	No	Quinn et al. (2012)
800	200–350	0.50 ^b	Yes	No	Bhakay et al. (2011)
10 ^a	360–500	60%	No	No	Juhnke et al. (2010)
1000	300	(-) ^c	Yes	No	Kim et al. (2010)
3600	500	46.7 g	No	No	Onoue et al. (2009)
1800–5500	500	(-) ^c	No	No	Fakes et al. (2009)
2930, 4400	500	(-) ^c	No	No	Deng et al. (2008)
5500	500	5.43 g	No	No	Dai et al. (2007)
5000	500	(-) ^c	No	No	Euler et al. (2004)

^aStirrer speed reported in (m/s).

^bVolume fraction or percentage in the milling chamber

^cValue not reported.

While evaluating the breakage kinetics yields empirical information about the impact of the process parameters, it does not yield a fundamental understanding or insights into the mechanisms of milling as a rate process, which entails a model to interpret and explain the observed kinetics. Various microhydrodynamic models have been developed to explain the dynamics of milling media in turbulent flow (Eskin et al., 2005a, b). Bilgili and co-workers (Afolabi et al., 2014; Li et al., 2015, 2017) have adapted these models and applied to WSMM of drug suspensions to gain fundamental process insights into the breakage kinetics, the impact of bead size, and viscous dampening of stabilizer solutions. However, such models have not been applied to WSMM of drug suspensions using CPS beads.

This study aims to investigate the impact of stirrer speed and CPS bead loading on the breakage kinetics—specific energy consumption during WSMM of griseofulvin (GF), a model poorly soluble drug, and compare CPS beads with YSZ beads at the highest bead loading. To this end, GF suspensions were milled at the stirrer speeds of 2000, 3000, and 4000 rpm with volumetric bead loading ranging from ~20% to 60%. Temporal evolution of the characteristic particle sizes was examined via laser diffraction off-line by measuring the particle size distribution (PSD) of milled samples taken at various milling times. Three characteristic time constants were defined and determined by interpolation/non-linear regression. Morphology of the milled GF particles was visualized by SEM imaging. X-ray powder diffraction (XRPD) was used to examine any solid-state changes during the milling. A microhydrodynamic model was used to interpret the observed kinetic behavior for various process parameters and bead materials. Finally, the selection of bead material is discussed in view of the observed breakage kinetics and specific power consumption.

1.3 Scope and Organization of Thesis

The objective of this thesis is to create nanoparticles of griseofulvin by use of wet stirred media milling. The following chapters outline the study of the impact of process parameters on the breakage kinetics using polymeric media and applying a microhydrodynamic model. Beyond this a material comparison is also evaluated using cross-linked polystyrene and yttrium stabilized zirconia media, in which a microhydrodynamic model is also applied. Chapter 2 contains the experimental aspects of the research, including materials and methods. Chapter 3 begins with the theoretical aspects of the microhydrodynamic model. After a brief explanation of the model, the results of the experiments are given and interpreted in chapter 4.

CHAPTER 2

EXPERIMENTAL

2.1. Preparation of Griseofulvin Nanosuspension

BP/EP grade micronized griseofulvin (GF) was purchased from Letco Medical (Decatur, AL, USA). GF is a BCS Class II drug and has a solubility of 8.9 $\mu\text{g/ml}$ at 25 °C (Li et al., 2017). Two stabilizers were used: a non-ionic cellulosic polymer, hydroxypropyl cellulose, (HPC SL grade, Nisso America, New York, NY, USA) and an anionic surfactant, sodium dodecyl sulfate (SDS, ACS grade, GFS chemicals, Columbus, OH, USA). HCC grade CPS beads with a nominal size of 400 μm were purchased from Norstone Inc. (Bridgeport, PA, USA) and Zirmil Y grade YSZ beads with a nominal size of 400 μm were purchased from Saint Gobain Zirpro (Mountside, NJ, USA). The 400 μm nominal bead size, which is one of the most commonly used sizes in wet stirred media milling, was selected considering an overview of the recent literature on bead sizes (Li et al., 2017) used in pharmaceutical wet media milling. The actual sizes of the CPS beads and the YSZ beads were measured to be 444 and 405 μm , respectively, using laser diffraction particle size analyzer (Helos/Rodos, Sympatec, NJ, USA) in dry dispersion mode. The actual median sizes were used in the microhydrodynamic model. De-ionized water was used in making all suspensions.

Selection of the stabilizer type–concentration was based on our extensive formulation studies in which GF suspensions were stabilized using a combination of HPC–SDS (Bilgili and Afolabi, 2012; Afolabi et al., 2014; Li et al., 2017). Not only did the use of 5% HPC and 0.5% SDS ensure the production of stable GF suspensions (Bilgili and Aflabi, 2012), but also this relatively viscous suspension formulation led to sufficiently

high power consumption when the CPS beads with low density were used, which enabled accurate determination of the energy consumption. About 230 g of pre-suspensions were prepared by dispersing 10% of micronized GF in a solution of 5% HPC and 0.5% SDS using a DLM 1638 shear mixer (Cat# 14-503, Fischer Scientific, Pittsburg, PA, USA) run at 300 rpm for about 120 minutes. All percentages are (w/w) with respect to water (200 g). The pre-suspensions were then milled for a total of 256 min in a Microcer wet stirred media mill (Netzsch Fine Particle Size Technology, LLC, Exton, PA, USA) under the conditions presented in Table 2. The mill is equipped with an 80 mL zirconia lined milling chamber V_m and zirconia rotor. Suspension were recirculated between the holding tank and the milling chamber at a volumetric flow rate Q of 126 mL/min, using a peristaltic pump (Cole-Palmer, Master Flex, Vermont Hills, IL, USA). Immediately exiting the milling chamber was a stainless-steel screen with nominal size of 200 μm . The screen ensured the beads were retained in the milling chamber and not be recirculated with the suspension. During milling, the suspension was cooled using a chiller (Model M1-0.25A-11HFX, Advantage Engineering, Greenwood, IN, USA) that circulated coolant through jackets located on the milling chamber and holding tank to ensure the temperature of the suspension never exceeded 35 °C. For the stirrer speed $\omega = 4000$ rpm and bead concentration $c > 0.3$, intermittent cooling was applied by periodically shutting down the mill, similar to Li et al., 2015 and Toziopoulou et al., 2017.



Figure 2.1 Image of the Netsch (Microcer) wet stirred media mill in recirculatory mode.

The (volumetric) fractional bead loading c in the milling chamber was varied from $\sim 20\%$ to 60% ; the maximum loading was limited by the theoretical random close packing of the spherical beads (63%). The stirrer (rotational) speed ω was varied from 2000, 3000, and 4000 rpm. The highest stirrer speed was chosen considering the maximum design speed of the mill, i.e., 4200 rpm. Stirrer speeds lower than 2000 rpm would not allow for enough size reduction within 256; hence, the minimum speed was set at 2000 rpm. Samples of the suspension during milling were taken at time intervals of 2^n minutes, where n is some integer, ($n = 0, 1, 2, \dots$). However, additional samples were taken at 24, 48, and 96 minutes in order to have enough data points that would aid in data fitting purposes in the analysis of breakage kinetics. Additionally, for the high energy/high bead loading conditions, $\omega = 4000$ rpm and $c = 0.594$ (Runs 12 and 15), samples were also taken at 20, 30, and 40 s.

These samples were taken due to fast breakage kinetics under these conditions; the median size d_{50} of the particles less was less than 1 μm within the first minute. Once milling was complete, the final suspensions were characterized as stated in Section 2.2.2. The milled suspensions were stored at 8 °C. After 7 days the suspensions were agitated and allowed to reach room temperature, after which particles sizes were measured again to investigate the stability of the milled suspensions.

Table 2.1 Process Parameters and Bead Material for Runs 1–15

Run No.	Stirrer Speed ω (rpm)	Bead Loading c (-)	Bead Material
1	2000	0.198	CPS
2	2000	0.298	CPS
3	2000	0.397	CPS
4	2000	0.594	CPS
5	3000	0.198	CPS
6	3000	0.298	CPS
7	3000	0.397	CPS
8	3000	0.594	CPS
9	4000	0.198	CPS
10	4000	0.298	CPS
11	4000	0.397	CPS
12	4000	0.594	CPS
13	2000	0.594	YSZ
14	3000	0.594	YSZ
15	4000	0.594	YSZ

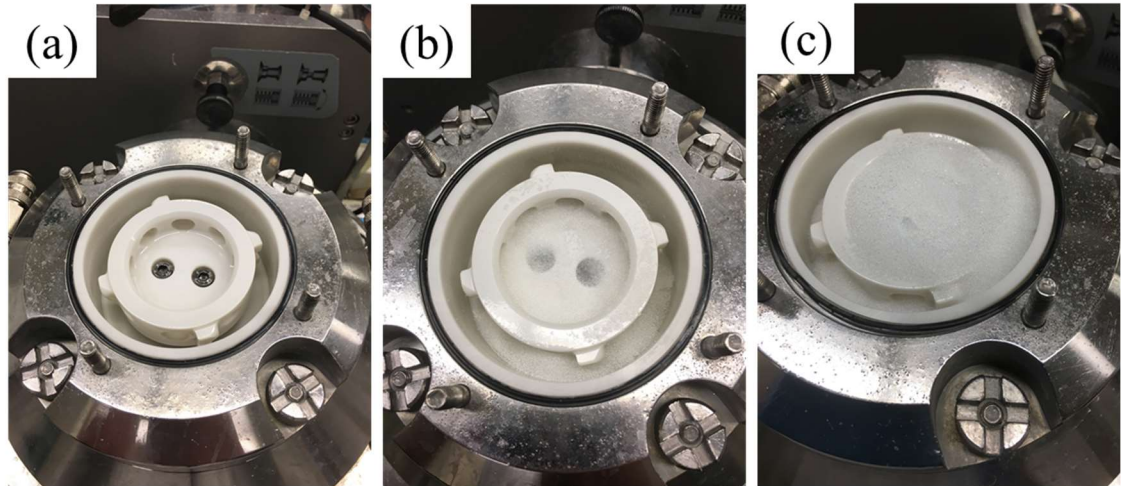


Figure 2.2 Images of the milling chamber (a) empty, (b) with CPS beads at a bead loading of $c = 0.198$ and (c) a bead loading of $c = 0.594$.

The average power consumption P involved in stirring the slurry (suspension and beads together), during the milling process was obtained from the control panel of the mill, which shows the cumulative energy consumption and milling time. The average power consumption per unit volume, which is shortly referred to as power consumption, was calculated as $P_w = P/V_m$. Power consumption from the shearing of the suspension itself ϵ_{ht} , i.e., suspension without beads, was also obtained from this control panel. In all cases, the power consumption in the absence of all material in the mill (no-load) was obtained and subtracted from P_w and ϵ_{ht} , in which ϵ_{ht} was found to be negligible.

2.2 Characterization Techniques

Particle size analysis of the milled GF suspensions was performed by laser diffraction using a LS 13-320 Beckman Coulter Instrument (Brea, Ca, USA). The polarized intensity differential scattering (PIDS) was maintained between 40% and 50% for all measurements. In each measurement the obscuration was not allowed to exceed 8%. The refractive indexes of GF and water were taken as 1.65 and 1.33, respectively. Prior to particle size

measurements, the samples taken at each time interval (~2 mL) were diluted with 5 mL of an HPC–SDS stock solution that consisted of the same concentrations as that of the suspension. The mixture was then vortexed at 1500 rpm for 1 min using a (Fischer Scientific Digital vortex mixer, Model No: 945415, NH, USA). For each sample the particle size was measured four times ($n = 4$); the average value was recorded along with the standard deviation.

CPS beads and YSZ beads were visualized using an Axio Scope.A1 polarized light microscope (Carl Zeiss Microscopy GmbH, Göttingen, Germany). Morphology of the milled particles from Runs 1, 12, and 15 was examined using a JEOL JSM 7900F field emission scanning electron microscope (SEM) (JEOL USA, Inc., Peabody, MA, USA) operated at 2 kV. 0.1 mL aliquot of each suspension sample was diluted up to 30 mL with deionized water and centrifuged (Compact II centrifuge, Clay Adams® Brand, Sparks, MD, USA) at 3200 rpm for 30 min in three steps to separate the drug from the aqueous phase with excess polymer. In every step, 10 mL deionized water was used for dilution and centrifuged for 10 min. After every 10 min, the aqueous phase with excess polymer was decanted and replaced with fresh deionized water and centrifuged for another 10 min. After centrifugation, an aliquot of the sample was mounted on top of a carbon specimen holder. This sample was placed into a desiccator for overnight drying under vacuum. The dried samples were then sputter coated with carbon using BAL-TEC MED020 (BAL-TEC, Balzers, Switzerland) to reduce possible charging during imaging.

Solid-state of as-received GF, HPC, SDS, a physical mixture of HPC–SDS–GF (unmilled), and milled, dried Run 1 and Run 12 suspensions was characterized using XPRD (PANalytical, Westborough, MA, USA), provided with Cu K α radiation ($\lambda = 1.5406 \text{ \AA}$).

Samples were scanned for a 2θ ranging from 5° to 40° at a scan rate of 0.165 s^{-1} . The apparent shear viscosities of the milled suspensions were measured using an R/S plus Brookfield Rheometer (Brookfield Engineering, Middleboro, MA, USA) at $25^\circ\text{C} \pm 0.5^\circ\text{C}$ with a coaxial cylinder (CC40). The milled suspension was then sheared at a shear rate from 0 to 1000 $1/\text{s}$ over a period of 60 s and μ_L was taken at the maximum shear rate in line with previous investigations (Berhnhart, et al, 1999). The density of the samples was determined by weighing 30 mL of each suspension three times $n = 3$ and taking the average. The density was then calculated by dividing the weight measured into the volume.

CHAPTER 3

THEORETICAL

3.1. Analysis of Breakage Kinetics

During milling, when particle breakage is the dominant mechanism as compared with particle aggregation, which will be the case for properly stabilized suspensions, the time-wise evolution of the median particle size d_{50} is characterized by an exponential decay with attainment of a limiting size given enough time, which is expressed as (Stražišar and Runovc, 1996; Varinot et al., 1999):

$$d_{50}(t) = d_{\text{lim}} + [d_{50}(0) - d_{\text{lim}}] \exp(-t / \tau_p) \quad (3.1)$$

where d_{lim} is the limiting median size value, τ_p is the characteristic process time constant, and $d_{50}(0)$ is the initial median particle size. Faster apparent breakage is represented by a lower τ_p value and corresponds to a more favorable (apparent) breakage rate. The exponential decay model was fit using a Levenberg-Marquardt algorithm to estimate d_{lim} and τ_p values. Initially, particle breakage was too fast in the first minute in contrast to the breakage observed throughout the entirety of the experiment. Therefore, the zero minute was discarded for fitting purposes and the median particle size of the first minute taken as the initial median size. This approach has been applied and justified in previous studies (Bilgili and Afolabi, 2012; Stražišar and Runovc, 1996; Varinot et al., 1999). Similarly, for Runs 12 and 15, 20 s data point was taken as the first point in fitting. Also, since d_{lim} should theoretically be less than the smallest particle size measured (256 min), a constraint was

imposed in which the d_{lim} was set to be less than the smallest particle size measured for each run.

3.2. Microhydrodynamic Analysis

The study of the dynamics of bead–bead collisions by the means of the transformation of turbulent kinetic energy into bead fluctuation kinetic energy is referred to as microhydrodynamics. Eskin et al. (2005a,b) developed a microhydrodynamic model to calculate the mean velocity of bead oscillation in well mixed suspensions using a granular energy balance (Gidaspow, 1994). For brevity, only notable features of the model are presented, which allows for a general understanding and readers are suggested to refer to Eskin et al. (2005a,b) for derivation and assumptions. The total power per unit volume, P_w , applied to a slurry of drug suspension and beads dissipates through three mechanisms, mathematically expressed as

$$P_w = \varepsilon_{visc} + \varepsilon_{coll} + \varepsilon_{ht} \quad (3.2)$$

$$P_w = \frac{54\mu_L c \theta R_{diss}}{d_b^2} + \frac{12}{d_b \sqrt{\pi}} (1 - k^2) \left[\frac{1 - 0.5c}{(1 - c)^3} \right] c^2 \rho_b \theta^{3/2} + \varepsilon_{ht} \quad (3.3)$$

where ε_{visc} is the energy dissipation rate due to both liquid–bead viscous friction and lubrication, ε_{coll} is the energy dissipation rate due to partially inelastic bead–bead collisions, and ε_{ht} is the energy spent on shearing the equivalent fluid (milled suspension). In Eq (3.3), μ_L is the apparent shear viscosity, c is the volumetric fractional bead concentration (bead loading). θ is the granular temperature defined as the bead–equivalent liquid relative root-

mean square velocity, R_{diss} is the effective drag coefficient, and d_b is the median size of the milling bead. k is the coefficient of restitution for bead–bead collisions: 0.9 for CPS (Cao et al., 2008) and 0.76 for YSZ (Tatsumi et al., 2009). ρ_b is the bead density: 1040 kg/m³ for CPS and 6000 kg/m³ for YSZ.

The equivalent liquid properties μ_L and ρ_b as well as the total power applied per unit volume P_w were measured. Given the measured liquid properties, P_w , and R_{diss} (see Appendix A for R_{diss} expressions), the granular temperature θ was calculated using MATLAB's `fsolve` function using Eq. (3.3). From the calculated θ , several microhydrodynamic parameters were then determined. Average bead oscillation velocity u_b and frequency of a single-bead oscillation ν were calculated using

$$u_b = \sqrt{\frac{8\theta}{\pi}} \quad (3.4)$$

$$\nu = \frac{24c}{d_b} \left[\frac{1-0.5c}{(1-c)^3} \right] \sqrt{\frac{\theta}{\pi}} \quad (3.5)$$

The microhydrodynamic model proposed by Eskin et al. (2005a) was advanced in a later paper (Eskin et al. 2005b) by including the elastic deformation of the beads along with the elastic-perfectly plastic deformation of the particles caught between the beads during collision. During milling, beads frequently collide due to their fluctuating motion in a slurry, which is characterized by θ , u_b , and ν , the beads capture and compress (deform) the particles. The maximum contact pressure at the center of the contact circle σ_b^{max} of the two colliding beads and the radius of the contact circle at the center of two colliding beads α_b are calculated as follows:

$$\sigma_b^{\max} = \frac{3F_b^n}{2\pi(\alpha_b)^2} \quad (3.6)$$

$$\alpha_b = \left[\frac{3(1-\eta_b^2)}{Y_b} R_b F_b^n \right]^{1/3} \quad (3.7)$$

where F_b^n is the normal force during collision of two elastic beads (see Appendix A). The average frequency of drug particle compressions a is the product of the probability of a drug particle to be captured between two colliding beads p and the frequency of a single bead oscillation ν given as:

$$a = p\nu \quad (3.8)$$

The energy dissipation rate attributed to the deformation of particles per unit volume Π is given by the expression:

$$\Pi = 2.23 \frac{c^2(2-c)}{(1-c)^3 \pi^{5/2} \varepsilon \sigma_y} \left[\frac{Y_b}{1-\eta_b^2} \right]^{18/15} \left(\frac{Y^*}{Y_p} \right)^\gamma \rho_b^{4/5} \frac{R_p}{(R_b)^2} \theta^{13/10} \quad (3.9)$$

where ε , σ_y , Y_b , η_b , Y^* , R_b , and R_p are the volume fraction of the drug in the suspension ($\varepsilon = 0.065$), contact pressure in a drug particle when fully plastic condition is reached, the Young's modulus of the beads, the Poisson ratio of the beads, the reduced elastic modulus of the bead-particle contact (Appendix A), radius of the bead, and the radius of the drug particle respectively. However, as a reliable value for σ_y is not available in the literature and our main interest is to examine the impact of the process variables and bead material

for the same drug (same σ_y for all Runs 1–15), instead of calculating Π , we calculated a pseudo energy dissipation rate, which is directly proportional to Π .

$$\Pi \cdot \sigma_y = 2.23 \frac{c^2(2-c)}{(1-c)^3 \pi^{5/2} \varepsilon} \left[\frac{Y_b}{1-\eta_b^2} \right]^{18/15} \left(\frac{Y^*}{Y_p} \right)^\gamma \rho_b^{4/5} \frac{R_p}{(R_b)^2} \theta^{13/10} \quad (3.10)$$

CHAPTER 4

RESULTS AND DISCUSSION

4.1. Effects of Wet Media Milling on Griseofulvin Particle Size and Morphology

Table 4.1 presents the characteristic particles sizes d_{10} , d_{50} (median size), and d_{90} after 256 min milling under various stirrer speed ω and CPS bead loading c as well as those obtained with YSZ beads at the highest bead loading. GF nanosuspensions with $d_{50} < 200$ nm were produced within 256 min using CPS beads for all stirrer speed–bead loadings except for $\omega = 2000$ rpm and $c < 0.4$ (Runs 1 and 2) and 3000 rpm and $c = 0.198$ (Run 5). Consider the initial d_{50} and d_{90} of the GF particles are 13.73 ± 0.087 and 33.96 ± 0.71 μm , this finding suggests a drastic size reduction during WSMM. The SEM images in Figure 4.1a and 4.1b corroborate the low extent of particle breakage in Run 1 with the lowest stirrer speed–bead loading, as signified by the similar morphology of particles to the as-received particles that have irregular and plate-like shapes. High extent of breakage under highly energetic milling conditions (Runs 12 and 15) caused formation of rounded/spherical particles. The SEM images qualitatively agree with the particle size range measured by laser diffraction (Table 4.1). A detailed analysis of Table 4.1 suggests that an increase in either beads loading or stirred speed led to finer median particle sizes after 256 min, while this effect seems to get weaker for $\omega > 2000$ rpm and $c > 0.3$.

Table 4.1 Particle Size Statistics of the Suspensions after 256 min of Milling and 7-day Storage

Run	Particle Sizes After Milling (μm)			Particle Sizes After 7-Day Storage (μm)		
No.	$d_{10} \pm \text{SD}^a$	$d_{50} \pm \text{SD}^a$	$d_{90} \pm \text{SD}^a$	$d_{10} \pm \text{SD}^a$	$d_{50} \pm \text{SD}^a$	$d_{90} \pm \text{SD}^a$
1	0.207 ± 0.021	1.53 ± 0.145	3.55 ± 0.141	0.235 ± 0.040	1.59 ± 0.186	3.82 ± 0.145
2	0.159 ± 0.007	0.318 ± 0.005	0.763 ± 0.069	0.170 ± 0.004	0.360 ± 0.057	0.645 ± 0.044
3	0.114 ± 0.003	0.176 ± 0.006	0.268 ± 0.021	0.116 ± 0.003	0.185 ± 0.003	0.264 ± 0.004
4	0.131 ± 0.001	0.161 ± 0.001	0.199 ± 0.002	0.129 ± 0.002	0.164 ± 0.001	0.211 ± 0.004
5	0.173 ± 0.013	0.301 ± 0.015	0.550 ± 0.042	0.168 ± 0.017	0.315 ± 0.012	0.525 ± 0.014
6	0.121 ± 0.000	0.175 ± 0.001	0.249 ± 0.001	0.121 ± 0.002	0.181 ± 0.001	0.251 ± 0.001
7	0.125 ± 0.000	0.168 ± 0.001	0.226 ± 0.000	0.129 ± 0.003	0.178 ± 0.009	0.242 ± 0.014
8	0.117 ± 0.001	0.144 ± 0.001	0.176 ± 0.001	0.117 ± 0.000	0.152 ± 0.012	0.177 ± 0.002
9	0.114 ± 0.001	0.175 ± 0.001	0.255 ± 0.000	0.119 ± 0.004	0.189 ± 0.009	0.268 ± 0.017
10	0.128 ± 0.001	0.169 ± 0.001	0.221 ± 0.001	0.129 ± 0.001	0.173 ± 0.000	0.224 ± 0.001
11	0.121 ± 0.000	0.149 ± 0.000	0.184 ± 0.001	0.129 ± 0.001	0.164 ± 0.001	0.203 ± 0.001
12	0.098 ± 0.002	0.122 ± 0.002	0.154 ± 0.005	0.102 ± 0.001	0.129 ± 0.001	0.157 ± 0.001
13	0.117 ± 0.001	0.144 ± 0.001	0.176 ± 0.001	0.126 ± 0.001	0.157 ± 0.003	0.199 ± 0.001
14	0.103 ± 0.002	0.128 ± 0.001	0.158 ± 0.001	0.110 ± 0.000	0.143 ± 0.001	0.178 ± 0.001
15	0.103 ± 0.001	0.128 ± 0.001	0.158 ± 0.001	0.109 ± 0.001	0.135 ± 0.000	0.167 ± 0.001

^aSD refers to standard deviation from the mean value of the specific particle size statistic obtained from multiple size measurements. It does not refer to the standard deviation of a fitted Gaussian particle size distribution.

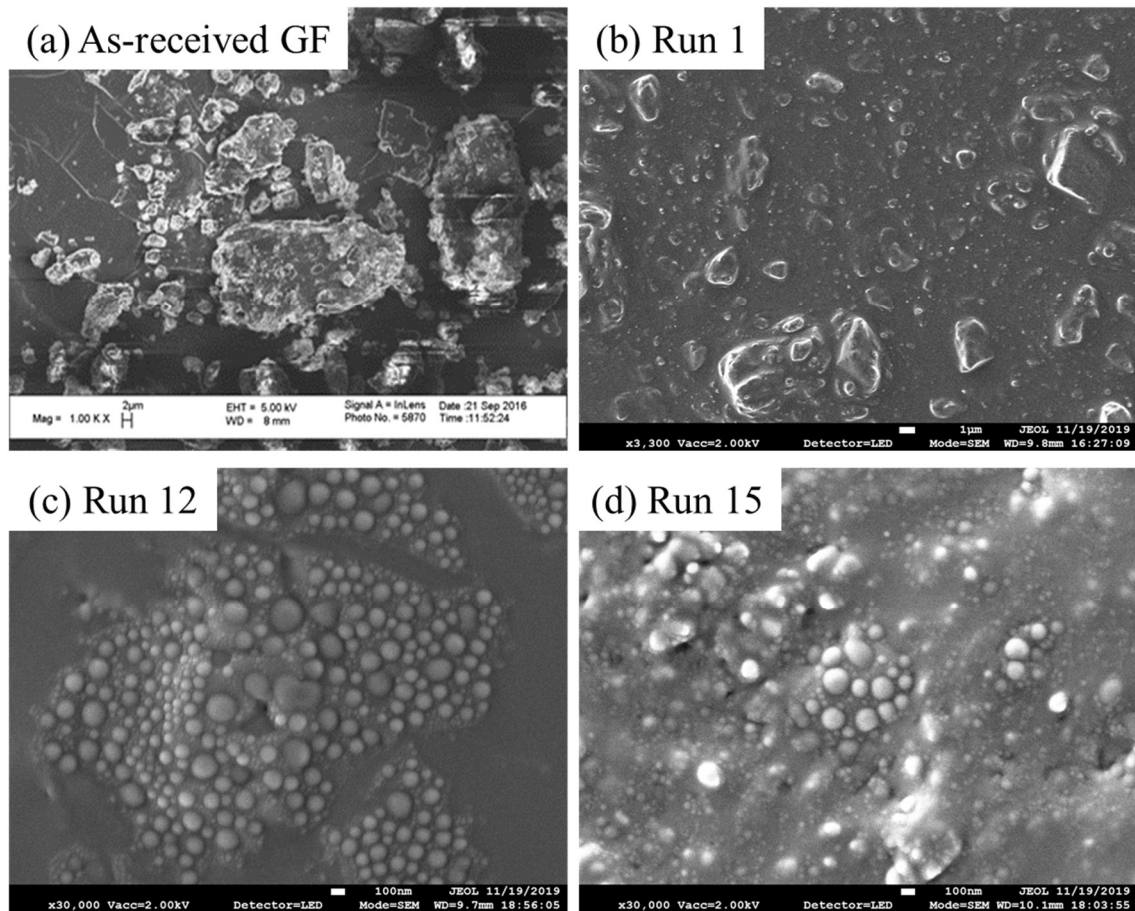


Figure 4.1 SEM images of (a) as-received GF particles and GF particles after 256 min of milling with (b) $\omega = 2000$ rpm with $c = 0.198$ using CPS beads (Run 1), (c) $\omega = 4000$ rpm with $c = 0.594$ using CPS beads (Run 12), and (d) $\omega = 4000$ rpm with $c = 0.594$ using YSZ beads (Run 15). Scale bar indicates 2 μm in (a), 1 μm in (b), and 100 nm in (c) and (d).

Short term physical stability of the suspensions was studied by measuring d_{10} , d_{50} , and d_{90} after a storage period of 7 days at 8°C. Relative deviation of the d_{10} , d_{50} , and d_{90} after milling from those after the 7-day storage period remained relatively low. The characteristic particles sizes did not change drastically after 7-day storage (Table 4.1). This suggests that aggregation and growth were effectively suppressed by making use of 5% HPC–0.5% SDS combination, which provides electrosteric stability to the GF suspensions (Bilgili and Afolabi, 2012). Long term physical stability was not evaluated in this study because the milled suspensions are intended for subsequent drying within a week to

produce drug nanocomposites (Li et al., 2016a; Bhakay et al., 2018). Reproducibility of wet media milling of griseofulvin with HPC–SDS has been well-established in previous studies (Bilgili and Afolabi 2012; Afolabi et al., 2014; Li et al., 2016a; Li et al., 2017); hence, will not be covered here for the sake of brevity.

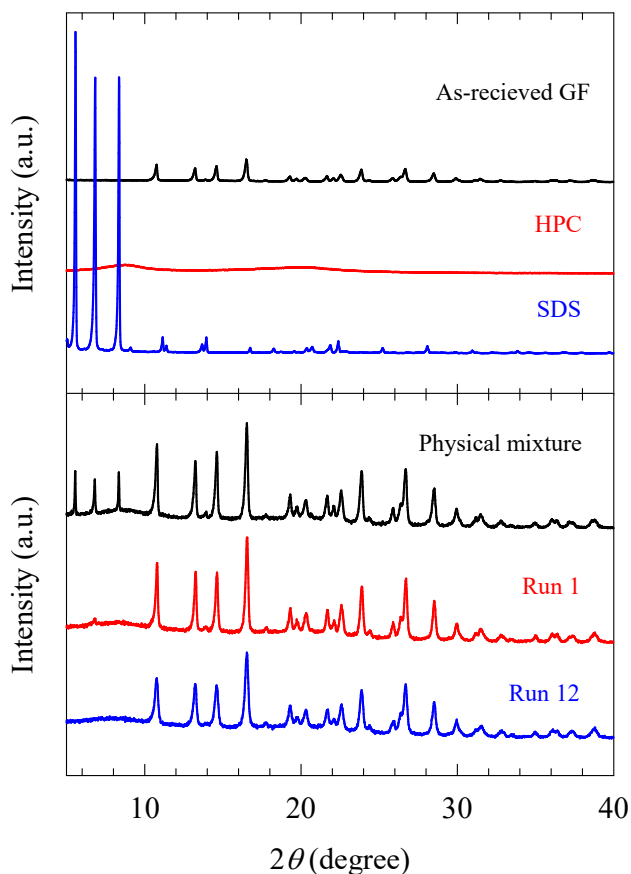


Figure. 4.2 XRPD diffractograms of (a) as-received GF, HPC, and SDS, and (b) unmilled physical mixture of GF–HPC–SDS, and dried, milled suspensions of Runs 1 and 12. Run 1 refers to the drug suspension milled at $\omega = 2000$ rpm with $c = 0.198$ and Run 12 refers to the drug suspension milled at $\omega = 4000$ rpm with $c = 0.594$.

During the wet milling process, stresses are applied to drug particles, which induces breakage. However, these stresses can also generate defects in the crystal structure of the drug and even amorphization (Feng et al., 2008). Figure 4.2 presents the XRPD diffractograms of as received GF, HPC, SDS, an un-milled physical mixture of HPC–SDS–

GF, along with the dried, milled suspensions from Runs 1 and 12. HPC diffractogram shows no peaks, pointing to the amorphous nature of HPC. GF and SDS are crystalline. The characteristic peaks of GF also appeared in the diffractograms of other samples containing GF, where SDS peaks disappeared in Runs 1 and 12 samples due to low concentration of SDS in the dried suspension samples and centrifugation in the preparation. The diffractograms of Runs 1 and 12 samples had similar GF peaks to that of the physical mixture, which implies that the crystallinity of GF was largely preserved after milling.

4.2. Impact of Process Parameters on Breakage Kinetics–Energy Consumption for Cross–Linked Polystyrene Beads

In order to quantify the apparent breakage kinetics, the temporal evolution of the GF median particle size was fitted to an exponential decay model (Eq. (3.1)) and the characteristic process time constant τ_p , whose inverse $1/\tau_p$ is equal to apparent breakage rate, was determined. Besides τ_p , as advocated in earlier studies (Afolabi et al., 2014; Li et al., 2017), two practical characteristic time constants were introduced: the time it takes for d_{50} to reach $0.5 \mu\text{m}$, i.e., t_{d50} , and the time it takes for d_{90} to reach $1 \mu\text{m}$, i.e., t_{d90} . These measures mathematically represent the particle sizes of a nanosuspension with majority of particles less than $1 \mu\text{m}$, which is required for effective improvement of drug dissolution rate (Kumar et al., 2014; Muller and Keck, 2004). MATLAB's pchip function, which uses a piecewise cubic Hermite polynomial interpolation, was used to calculate t_{d50} and t_{d90} (full data presented in Table B.1 of Appendix B). The specific energy consumption during t_{d50} , i.e., E_{td50} , and the specific energy consumption during t_{d90} , i.e., E_{td90} , were determined by the following expressions:

$$E_{td50} = \frac{P_w V_m t_{d50}}{m_D} \quad (4.1)$$

$$E_{td90} = \frac{P_w V_m t_{d90}}{m_D} \quad (4.2)$$

where m_D is the mass of the drug in the suspension (20 g). 3D mesh plots for P_w , E_{td50} , and E_{td90} over the ω - c space were generated using cubic interpolation in MATLAB (full data presented in Table B.2 of Appendix B). Using Eq. (3), a merit score was calculated for each milling run based on the operational principle that a milling process should have low cycle time and low specific energy consumption for a defined drug particle fineness.

$$\text{Merit score} = \frac{A}{E_{td50} t_{d50}} \quad (4.3)$$

Here, the merit constant A is a normalizing constant arbitrarily set at 10^6 J·min/g for proper scaling of the merit score and the associated figures.

4.2.1. Impact of Stirrer Speed and Bead Loading

The temporal evolution of d_{50} and d_{90} of the GF particles is presented in Figure 4.3. For more clarity and discernment of the impact of varying process parameters, all plots were produced in log-log scale with the removal of the initial time point ($t = 0$ min). In general, both d_{50} and d_{90} decreased monotonically in time, within experimental accuracy, suggesting particle breakage was the dominant mechanism and aggregation was largely suppressed during the milling. As mentioned in Section 4.1, this could be explained by the effective stabilization provided by 5% HPC–0.5% SDS. As milling progressed, depending on the

breakage kinetics and given enough time, the median size began to plateau towards a steady-state particles size, which is known as the apparent grinding limit (Knieke et al., 2009, 2013). This grinding limit can be explained by two factors; first is the lower probability of capturing smaller particles, which were naturally generated as milling progresses, between two colliding beads (Eskin et al., 2005b), as explained by Eq. (A7) of Appendix A. The second factor is the lower breakage probability of nanoparticles compared to microparticles (Bilgili et al., 2006) besides the small extent of aggregation. Figure 3 also illustrates that the grinding limit was attained earlier when either a higher stirrer speed or a higher bead loading was used. An increase in bead loading at a given stirred speed yielded finer particles, as signified by the lower d_{50} and d_{90} values, at a given time. Also, for the same bead loading, a comparison of Figure 4.3a, 4.3b, and 4.3c suggests that an increase in stirrer speed yielded finer particles at a given time. All these observations qualitatively point to faster breakage at higher stirrer speed–bead loading. For Runs 1–3, a delay in the reduction of particles sizes was observed. In these specific runs, irregular flow was observed at the outlet of the mill. Reversing the pump for a short duration (few seconds) multiple times during the first few minutes relieved this problem, suggesting clogging at the screen was occurring. This was not surprising as the particle breakage was extremely slow at 2000 rpm, causing accumulation of unbroken large particles, unless a bead loading of ~60% ($c = 0.594$) was used.

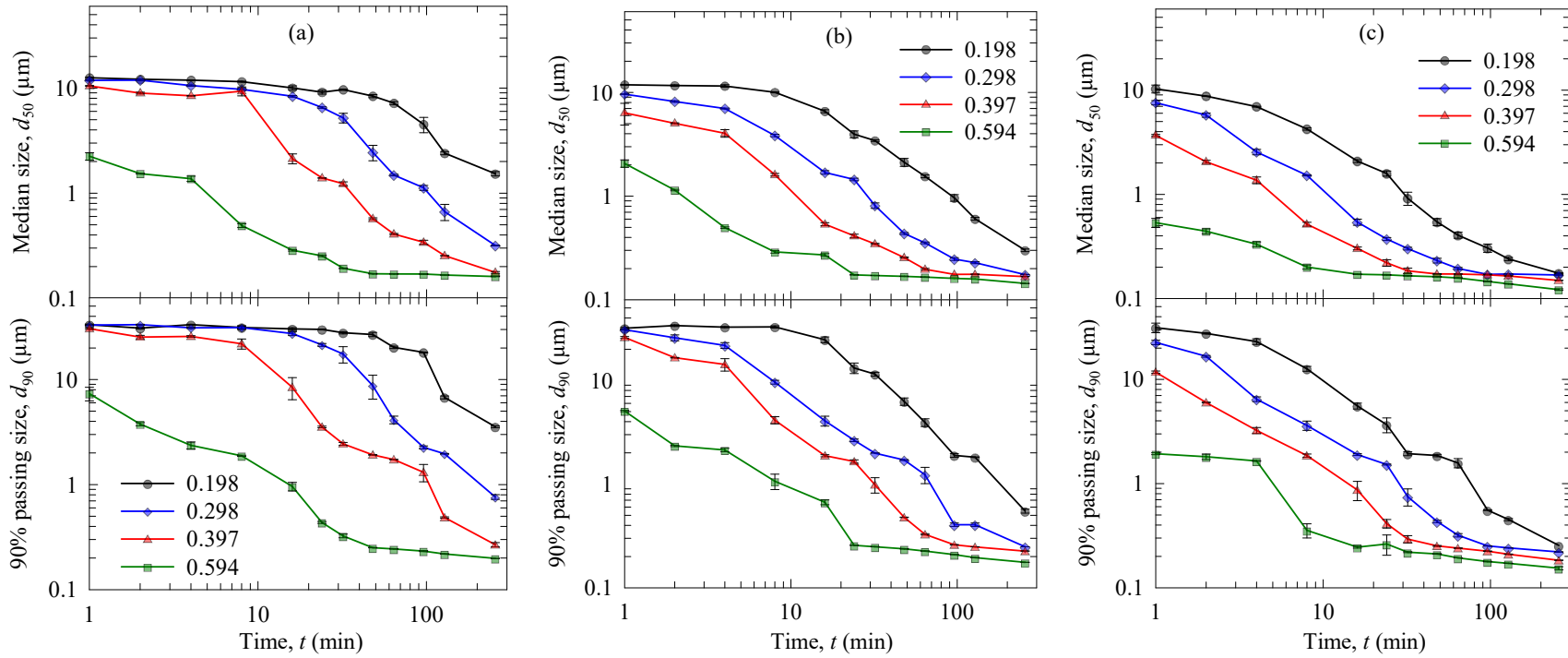


Figure 4.3 Effects of CPS bead loading c on the time-wise evolution of d_{50} and d_{90} during wet stirred media milling of GF particles at various stirrer speeds: (a) $\omega = 2000$ rpm, (b) $\omega = 3000$ rpm, and (c) $\omega = 4000$ rpm. At $t = 0$, the GF particles had $d_{50} = 13.73 \pm 0.087$ μm and $d_{90} = 33.96 \pm 0.711$ μm .

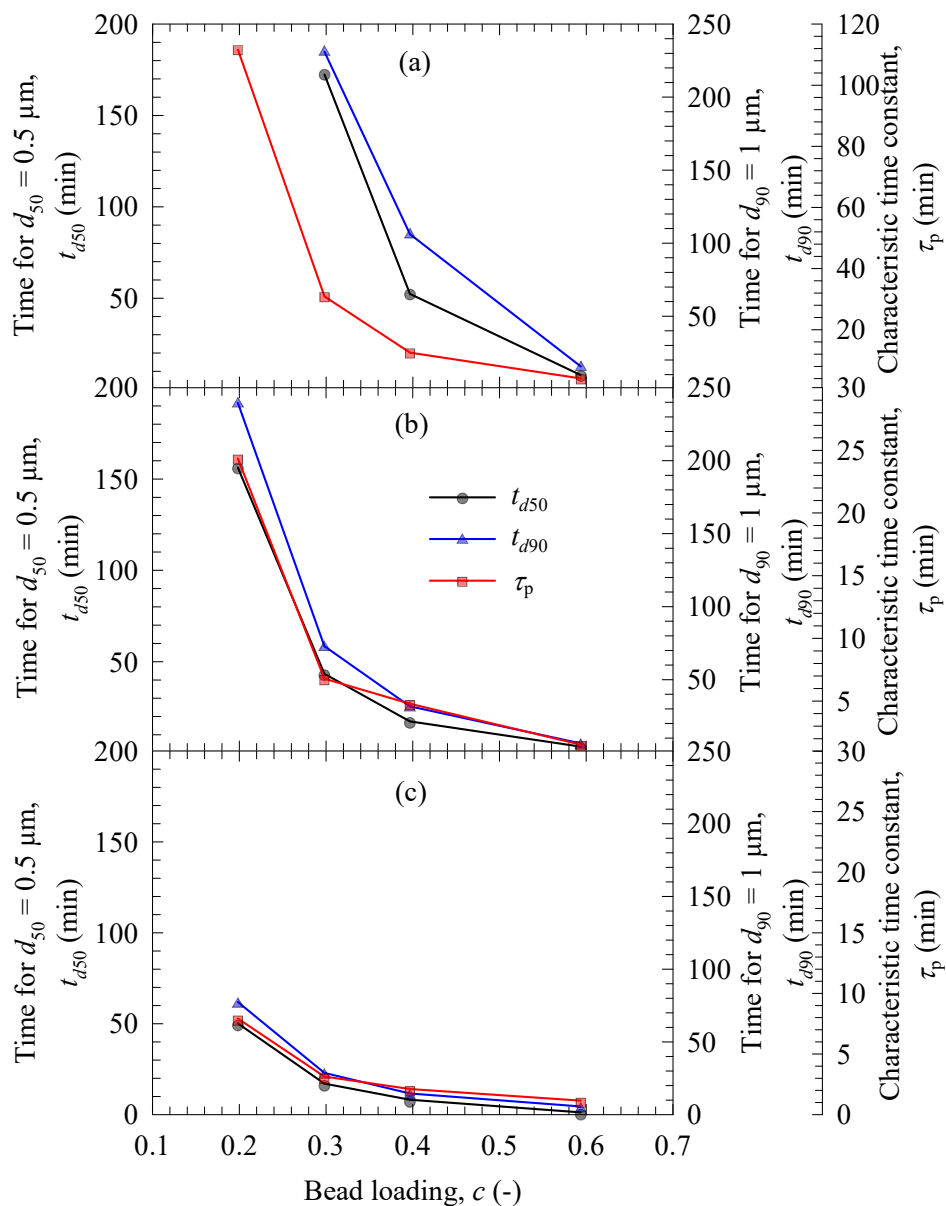


Figure 4.4 Effects of CPS bead loading c on characteristic milling times t_{d50} , t_{d90} , and τ_p at various stirrer speeds: (a) $\omega = 2000$ rpm, (b) $\omega = 3000$ rpm, and (c) $\omega = 4000$ rpm. Note, for $\omega = 2000$ rpm and $c = 0.198$, d_{50} and d_{90} did not reach $0.5 \mu\text{m}$ and $1 \mu\text{m}$, respectively.

Figure 4.4 illustrates that all characteristic time constants t_{d50} , t_{d90} , and τ_p decreased monotonically upon an increase in CPS bead loading. At a given CPS bead loading, they were reduced by an increase in stirrer speed. Not only did the three characteristic time constants accord well with the qualitative trends observed in Figure 4.3, but also, they

described the impact of stirrer speed–bead loading in a consistent manner. Moreover, these observations and general trends agree well with those regarding the impact of stirrer speed–bead loading for YSZ beads (Afolabi et al., 2014). It should be noted that for Run 1 (the lowest stirrer speed–bead loading), t_{d50} and t_{d90} values are not reported because d_{50} and d_{90} did not reach 0.5 μm and 1 μm , respectively.

Figures 4.5, 4.6, and 4.7 present 3D mesh plots, respectively, for the average power consumption per unit volume P_w , specific energy consumption during t_{d50} to reach 0.5 μm , i.e., E_{td50} , and specific energy consumption during t_{d90} to reach 1 μm , i.e., E_{td90} , as a function of stirrer speed ω and CPS bead loading c . An increase in either stirrer speed or bead loading caused an increase in the specific power consumption (Figure 4.5). The impact of CPS bead loading on P_w can be explained by an increase in the slurry viscosity μ_m as the slurry density ρ_m remained almost unchanged when the CPS bead loading was increased. The readers are referred to Table B.3 Appendix B, which presents the slurry density ρ_m and the slurry viscosity μ_m values calculated based on the following expressions (Gillies and Shook, 2000)

$$\rho_m = \rho_b c + \rho_L (1 - c) \quad (4.4)$$

$$\mu_m = \mu_L [1 + 2.5c + 10c^2 + \exp(20c)] \quad (4.5)$$

The invariance of the slurry density ρ_m to higher CPS bead loading is attributed to the similar values of the density of the milled drug suspension ρ_L and the density of the CPS beads ρ_b . It is well-known from the well-established correlations that the power

consumption in wet stirred media mills is higher for denser or more viscous slurries and slurries mixed at higher speeds (see e.g. Mannheim, 2011). Surprisingly, the specific energy consumption to reach the desired particle sizes, E_{td50} and E_{td90} , exhibited an opposite trend as compared with the power consumption (Figures 4.6 and 4.7). Although an increase in either stirrer speed or bead loading resulted in more power consumption, it also led to faster breakage and lower values of t_{d50} and t_{d90} , which led to lower specific energy consumption. Overall, Figures 4.6 and 4.7 suggest that more intense (higher power consumption) milling conditions entail less expenditure of specific energy to produce a d_{50} of 0.5 μm and a d_{90} and 1 μm , owing to the resultant faster breakage. The merit score of the milling runs presented in Figure 4.8 suggests that wet stirred media milling is most favorable, i.e., having the lowest production time and the lowest specific energy consumption, under the most intense milling conditions, i.e., the highest stirrer speed and the highest bead loading.

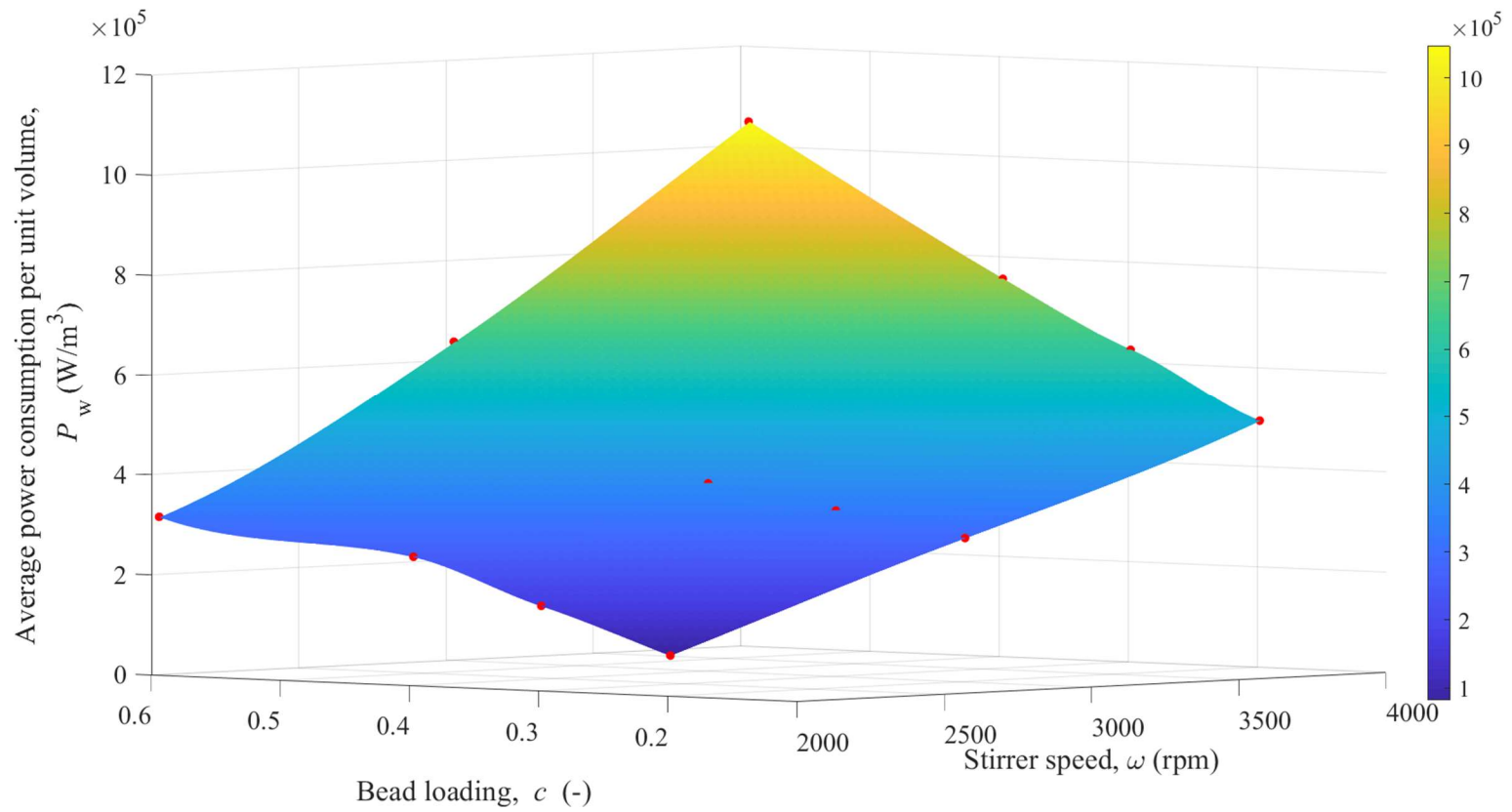


Figure 4.5 Effects of stirrer speed ω and CPS bead loading c on the average power consumption per unit volume P_w for Runs 1–12.

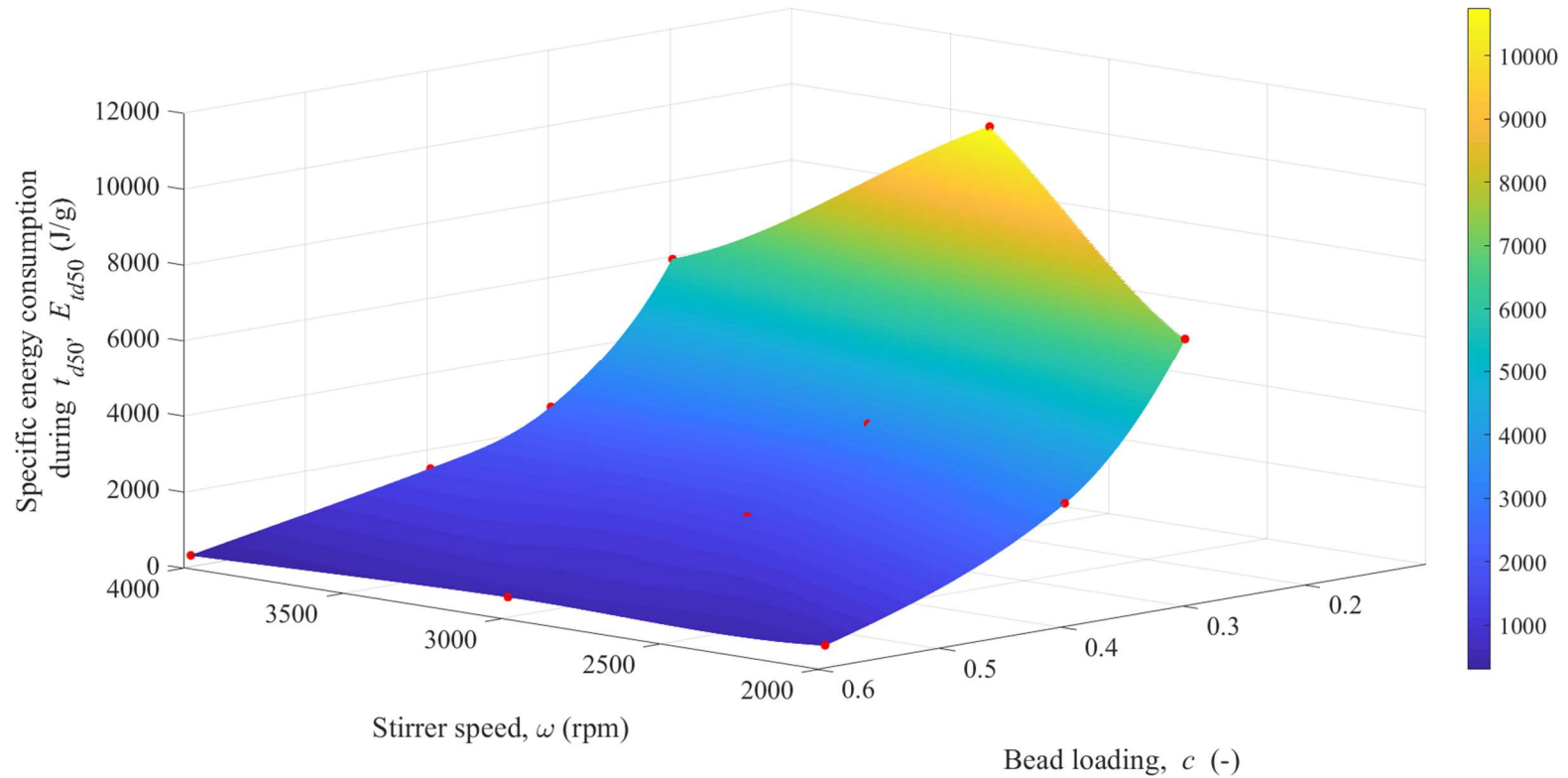


Figure 4.6 Effects of stirrer speed ω and CPS bead loading c on the specific energy consumption during t_{d50} (E_{d50}) for Runs 2–12.

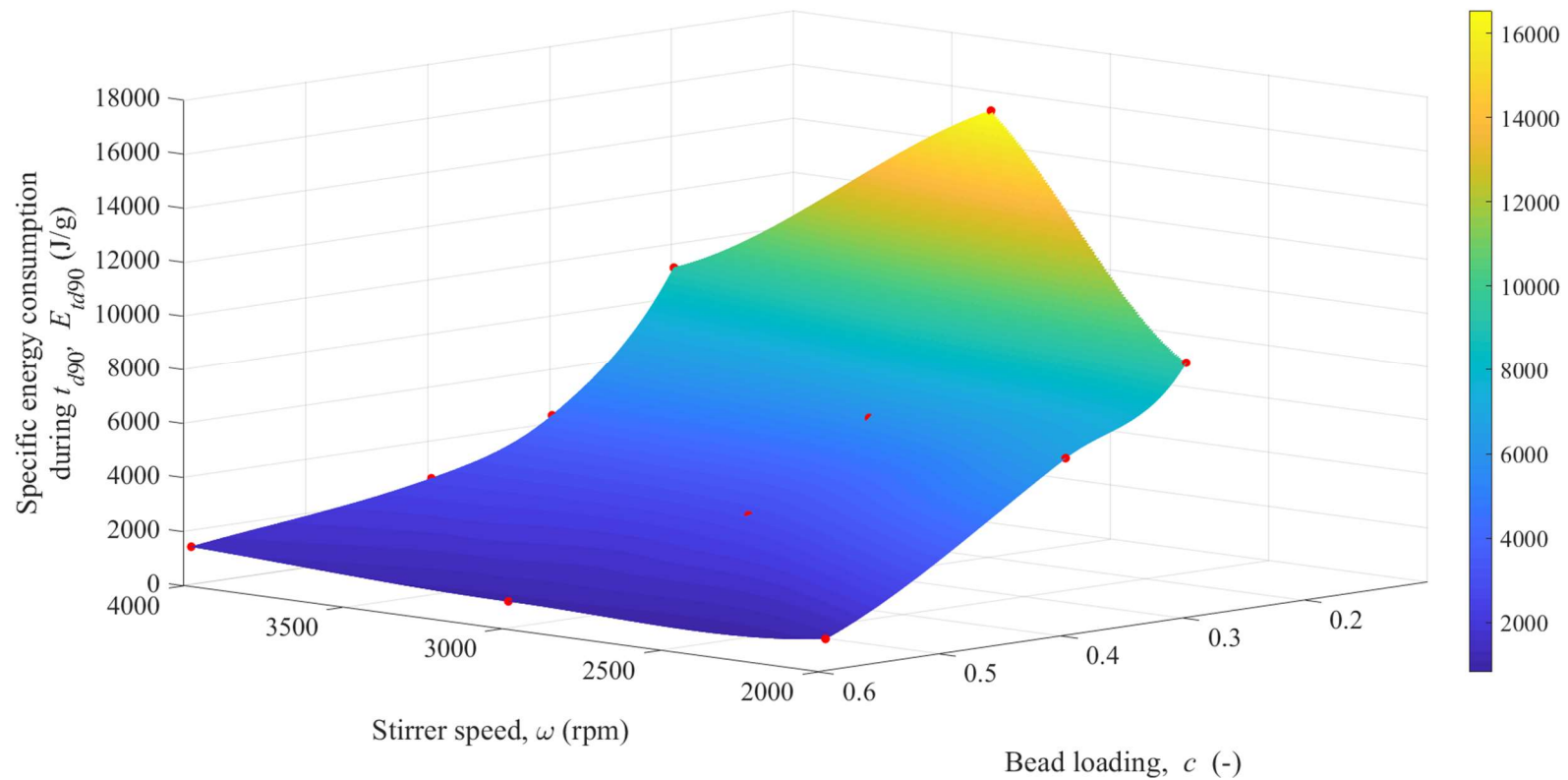


Figure 4.7 Effects of stirrer speed ω and CPS bead loading c on the specific energy consumption during t_{d90} ($E_{t_{d90}}$) for Runs 2–12.

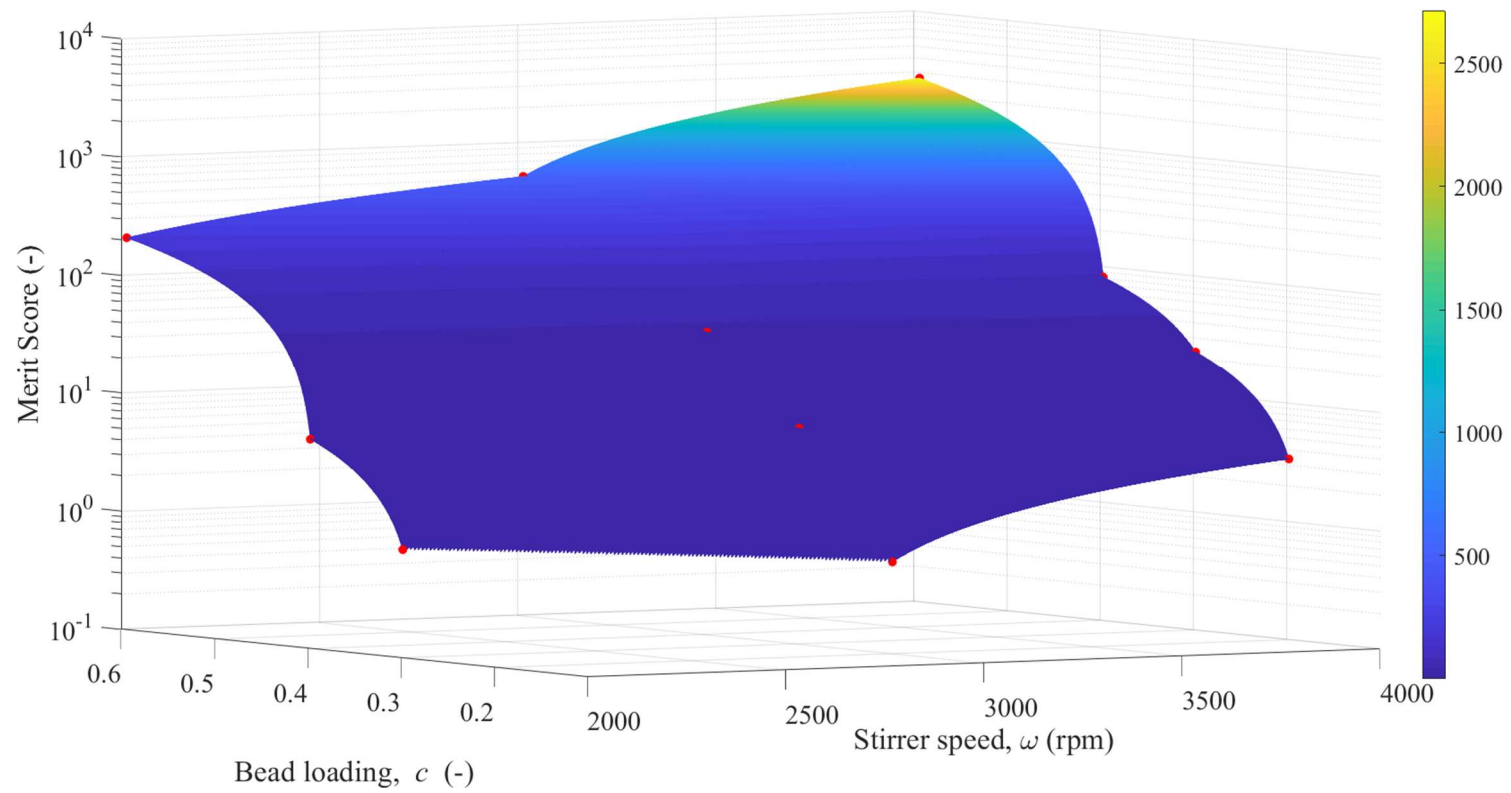


Figure 4.8. Effects of stirrer speed ω and CPS bead loading c on the Merit score (-) for Runs 2–12.

4.2.2. Microhydrodynamic Analysis of the Impact of Process Parameters for Cross-Linked Polystyrene Beads

Figures 4.9 and 4.10 present the variation of several microhydrodynamic parameters as function of the bead loading at various stirrer speeds. Interestingly, two counteracting effects of the bead loading on the breakage were observed. First, as the bead concentration increased, the fluctuating motion of the beads slowed down, as signified by the lower granular temperature θ (Figure 4.9) because the energy losses through viscous frictional losses and inelastic collisions of higher number of beads overshadowed the increase in the power consumption (refer to Figure 4.5). The average oscillation velocity u_b followed a similar trend to that of θ (Figure 4.9). This decrease in the bead oscillation velocity resulted in less stressful/forceful bead-bead collisions, which ultimately led to a decrease in maximum contact pressure σ_b^{\max} (Figure 4.10). All the above effects of the bead loading are unfavorable for particle breakage. However, an increase in the number of beads generated a higher frequency of single bead oscillation ν , which led to more frequent drug particles compression a (Figure 4.10). This effect of the bead loading is favorable to particle breakage.

The overall effect of the bead loading can be viewed as a competition between the intensity of stressful events (σ_b^{\max}) generated and the number/frequency of the stressful events (a) that occurred. As the favorable impact of the bead loading on a are more drastic than the unfavorable impacts of the bead loading on σ_b^{\max} , the overall impact of the bead loading was favorable in terms of particle breakage, which explains the faster breakage observed at the higher bead loading (refer to Figure 4.4). Another likely explanation is that the breakage rate is affected more by the average frequency of drug particle compressions

than the maximum contact pressure σ_b^{\max} provided that σ_b^{\max} is not too low. Afolabi et al. (2014) and Li et al. (2017) proposed for YSZ beads that the dominant effect associated with a on the breakage kinetics as compared with σ_b^{\max} emerges from a damage mechanism called contact fatigue for the drug particles when they are captured multiple times by the colliding beads. Multiple, frequent compressions of the drug particles with low stress intensity can cause nucleation of permanent structural defects that lead to crack initiation; the growth of cracks eventually results in particle fracture (Bilgili et al., 2006; Eskin et al., 2005a). Thus, it is likely that GF particles may break at lower stresses than their static fracture strength values, thus making their breakage rate more sensitive to the average frequency of drug particle compressions a than the maximum bead contact pressure σ_b^{\max} under the specific milling conditions explored here. This mechanism needs further investigation. Also, the overall impact of the bead loading may be seen from Figure 10, which illustrates the monotonically increasing pseudo energy dissipation rate stemming directly from the deformation of the drug particles. Finally, a cursory look at Figures 4.9 and 4.10 indicates that at a given beads loading c , upon an increase in the stirrer speed, all microhydrodynamic parameters took on higher values, which in turn signifies the occurrence of more forceful/stressful bead–bead collisions and drug particle compression events at a higher frequency, which together explains the faster breakage rate at the higher speeds.

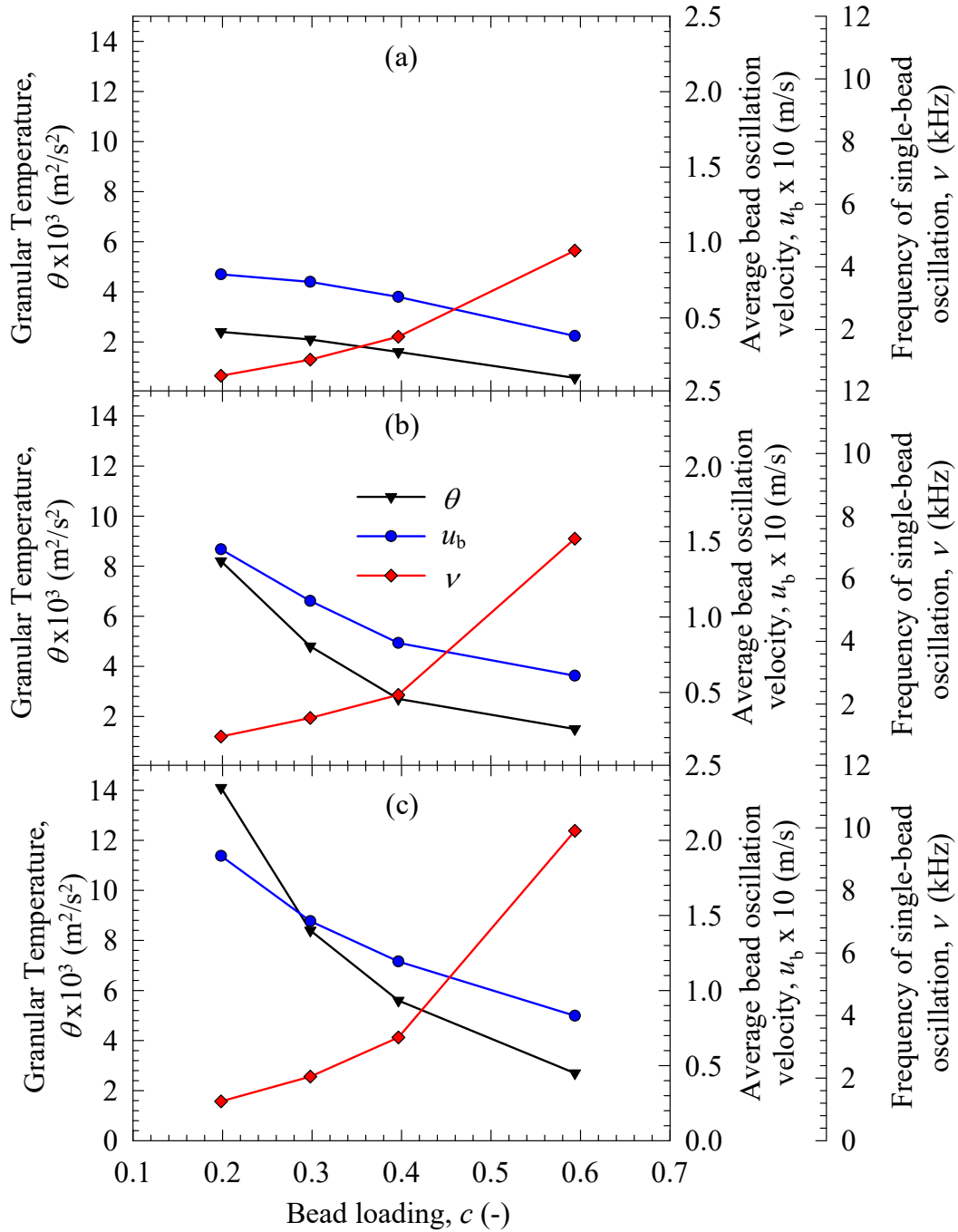


Figure 4.9 Effects of CPS bead loading c on granular temperature θ , average bead oscillation velocity u_b , and frequency of single-bead oscillation ν at various stirrer speeds: (a) $\omega = 2000$ rpm, (b) $\omega = 3000$ rpm, and (c) $\omega = 4000$ rpm (Runs 1–12).

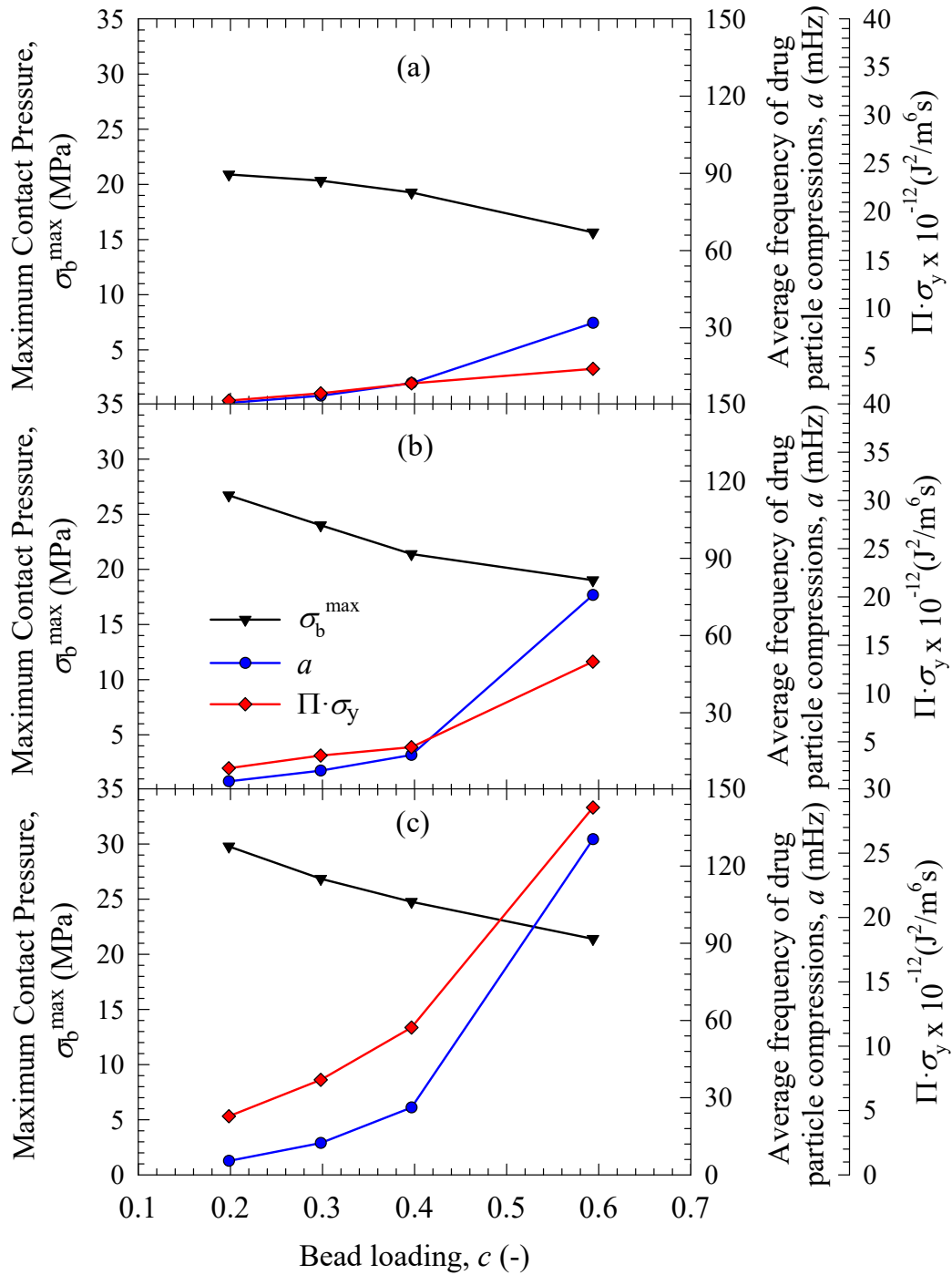


Figure 4.10. Effects of CPS bead loading c on the maximum contact pressure σ_b^{\max} , the average frequency of drug particle compressions a , and the pseudo energy dissipation rate $\Pi \cdot \sigma_y$ at various stirrer speeds: (a) $\omega = 2000$ rpm, (b) $\omega = 3000$ rpm, and (c) $\omega = 4000$ rpm (Runs 1–12).

4.3. Impact of Media Material: A Comparative Analysis

As the selection of milling media material could greatly affect the breakage kinetics–energy consumption in WSMM Here, we performed a systematic comparison of CPS and YSZ beads (media) using WSMM. This was done by comparing the outcomes of six experiments, for CPS Runs 4, 8, and 12 and for YSZ Runs 13–15 in which the bead performance was compared at the highest c value of 0.594. This c was chosen for the comparison as it showed the fastest breakage and produced the lowest τ_p at any given stirrer speed during the CPS experiments in Section 4.2. To make the comparison fair, we kept the drug/stabilizer concentrations the same, similar to those in Section 4.2. The optical microscope images show that both CPS and YSZ beads have identical shapes; they are

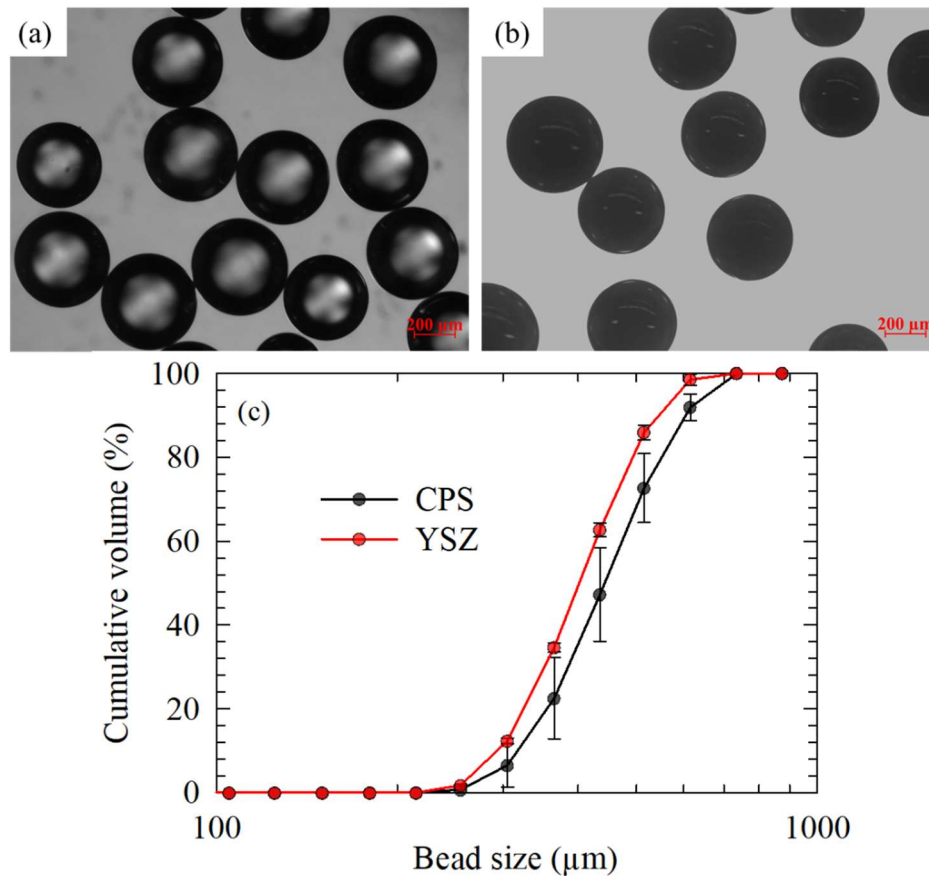


Figure 4.11 Optical microscope image of 400 μm nominal sized (a) CPS beads (measured median size: 444 μm) and (b) YSZ beads (measured median size: 405 μm) and (c) particle size distributions of the beads.

spherical with smooth surfaces (Figure 11a and 11b). Having identical nominal sizes labeled by their suppliers, i.e., 400 μm , YSZ beads are slightly smaller than CPS beads: median size of 405 μm vs. median size of 444 μm (Figure 11c). Note that the actual median sizes as opposed to the nominal sizes were used in the microhydrodynamic analysis.

4.3.1. Impact of Media Material on Breakage Kinetics

Figure 4.12 shows the temporal evolution of the d_{50} and d_{90} of GF particles using both CPS and YSZ media using WSMM. As observed in Section 4.2.1 when stirrer speed was increased, both d_{50} and d_{90} decreased monotonically for both CPS and YSZ, and they tended to plateau for all runs. The profiles in Figure 4.12 qualitatively depict that the YSZ beads achieved faster breakage of the drug particles than the CPS beads. The characteristic time constants t_{d50} , t_{d90} , and τ_p presented in Figure 4.13 quantitatively describe the faster breakage kinetics with an increase in stirrer speed and faster breakage with YSZ beads as indicated by the lower values of t_{d50} , t_{d90} , and τ_p . Also presented in Figure 13 are the specific energy consumptions E_{td50} , E_{td90} , and merit scores of CPS and YSZ as a function of the stirrer speed. Due to the higher density of YSZ beads ($\rho_b = 6000 \text{ kg/m}^3$) and its slurries as compared with that of CPS beads ($\rho_b = 1040 \text{ kg/m}^3$), which is in line with Eq. (4.4), the runs with YSZ beads had much higher power consumption than CPS beads (refer to Table B.4 in Appendix B), and the power consumption drastically increased with an increase in the stirrer speed for a given bead material. Although YSZ beads also led to lower t_{d50} , t_{d90} , and τ_p or faster breakage, the drastic increase in the power consumption P_w led to a higher specific energy consumption (E_{td50} and E_{td90}) for YSZ beads than CPS beads, except for E_{td50} at $\omega = 2000 \text{ rpm}$. Nonetheless, the relative difference of specific breakage

consumption between YSZ and CPS beads were much lower than the relative difference of the power consumption between them.

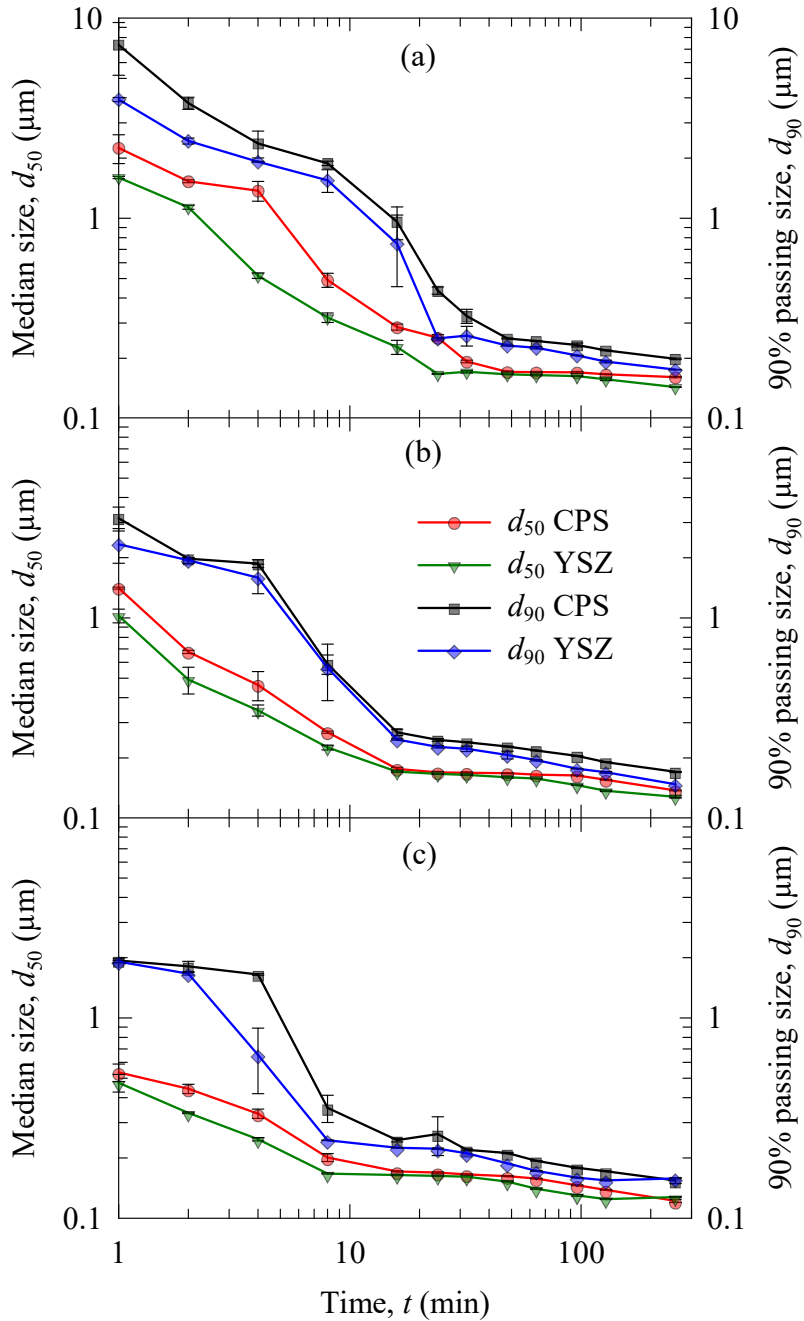


Figure 4.12 Effects of bead material, i.e., CPS vs. YSZ, on the evolution of the median size of GF particles beads at a fixed bead loading of $c = 0.594$ and various stirrer speeds: (a) $\omega = 2000$ rpm, (b) $\omega = 3000$ rpm, and (c) $\omega = 4000$ rpm. . At $t = 0$, the GF particles had $d_{50} = 13.73 \pm 0.087 \mu\text{m}$ and $d_{90} = 33.96 \pm 0.711 \mu\text{m}$.

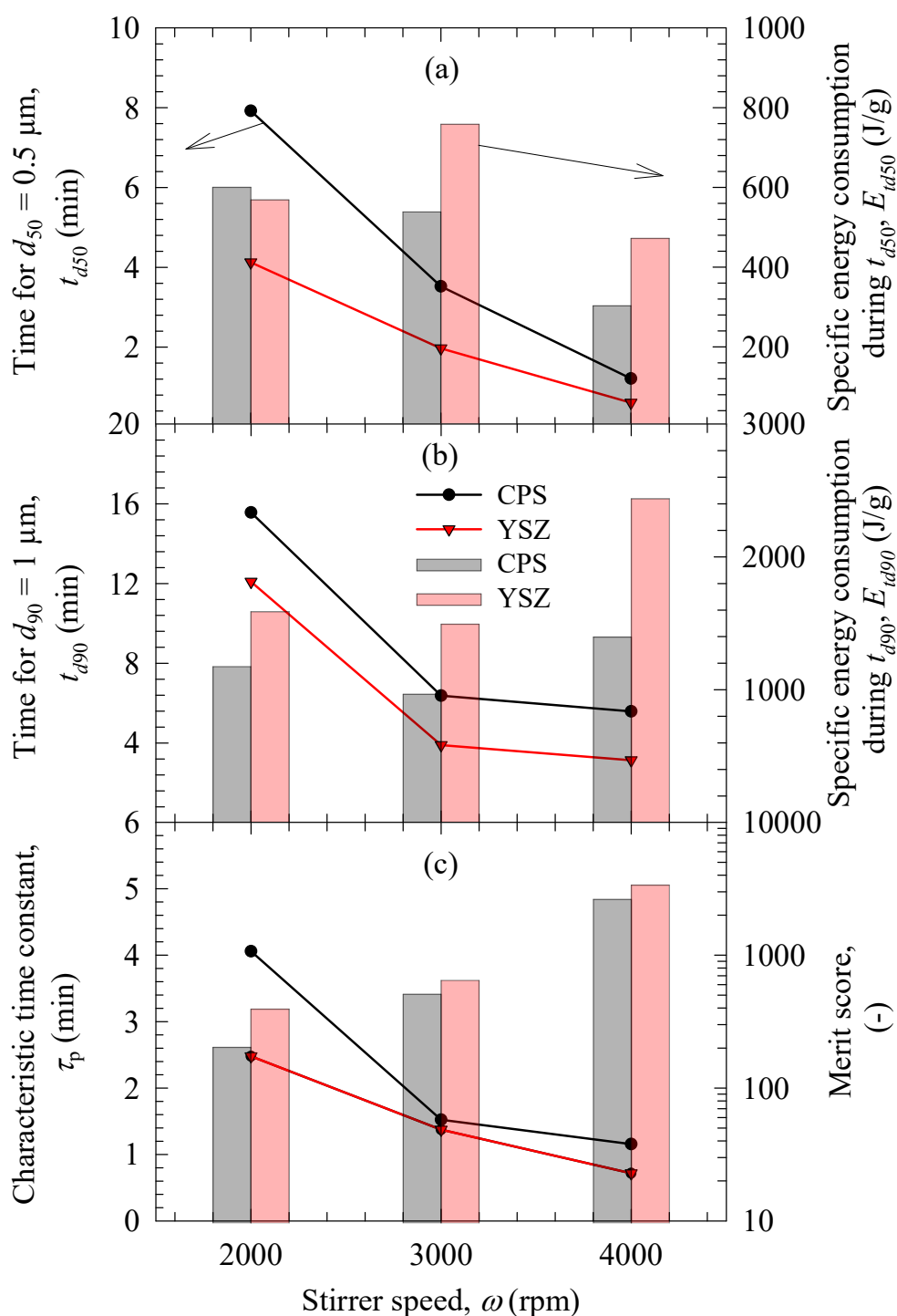


Figure 4.13 Effects of stirrer speed on the characteristic milling times, energy consumptions, and merit score: (a) t_{d50} and E_{td50} (b) t_{d90} and E_{td90} , and (c) τ_p and merit score when CPS and YSZ beads were used. Lines illustrate characteristic times; bars illustrate energy consumptions and merit score.

4.3.2. Microhydrodynamic Analysis of the Impact of Media Material in WSMM

As described previously in Section 4.2.2 for CPS beads, when the stirrer speed was increased, all microhydrodynamic parameters increased monotonically for both CPS and YSZ beads, which is quite favorable from the viewpoint of particle breakage and kinetics: more intense/forceful bead–bead collisions with higher frequency. Since more power was applied to the YSZ beads during the milling than the CPS beads at the same stirrer speed, as explained in Section 4.3.1., in general, this resulted in more frequent bead fluctuations with higher kinetic energy and oscillation velocity, i.e., higher θ and u_b (Figure 4.14a and 14b) as well as higher frequency of drug particle compressions a (Figure 4.14c). The differences in these parameters between YSZ beads and CPS beads were more pronounced at the higher speeds. With higher fluctuating kinetic energy, YSZ beads having higher modulus of elasticity ($Y_b = 200$ GPa, see Appendix A) than the CPS beads ($Y_b = 1.5$ GPa) resulted in a higher maximum contact pressure σ_b^{\max} (Figure 14d) and a lower radius of contact circle than the CPS beads (Figure 4.14e) at the same stirrer speed. To the best knowledge of the authors, this is the first quantitative verification of the commonly held notion that softer beads (CPS) should allow for a larger contact circle than harder beads (YSZ), which is advantageous to capturing fine drug particles during the milling. However, despite this advantage of the CPS beads, due to their lower θ and u_b , their use led to smaller frequency of drug particle compressions a than the YSZ beads (except at $\omega = 2000$ rpm). For $\omega = 2000$ rpm, CPS beads yielded a slightly higher value of a than YSZ; yet they caused slower breakage. This can possibly be explained by the lower σ_b^{\max} and $\Pi \cdot \sigma_y$ generated by CPS at the lowest stirrer speed used here. Finally, Figure 4.14f indicates

higher pseudo energy dissipation rate stemming directly from the deformation of the drug particles when YSZ beads were used as opposed to CPS beads.

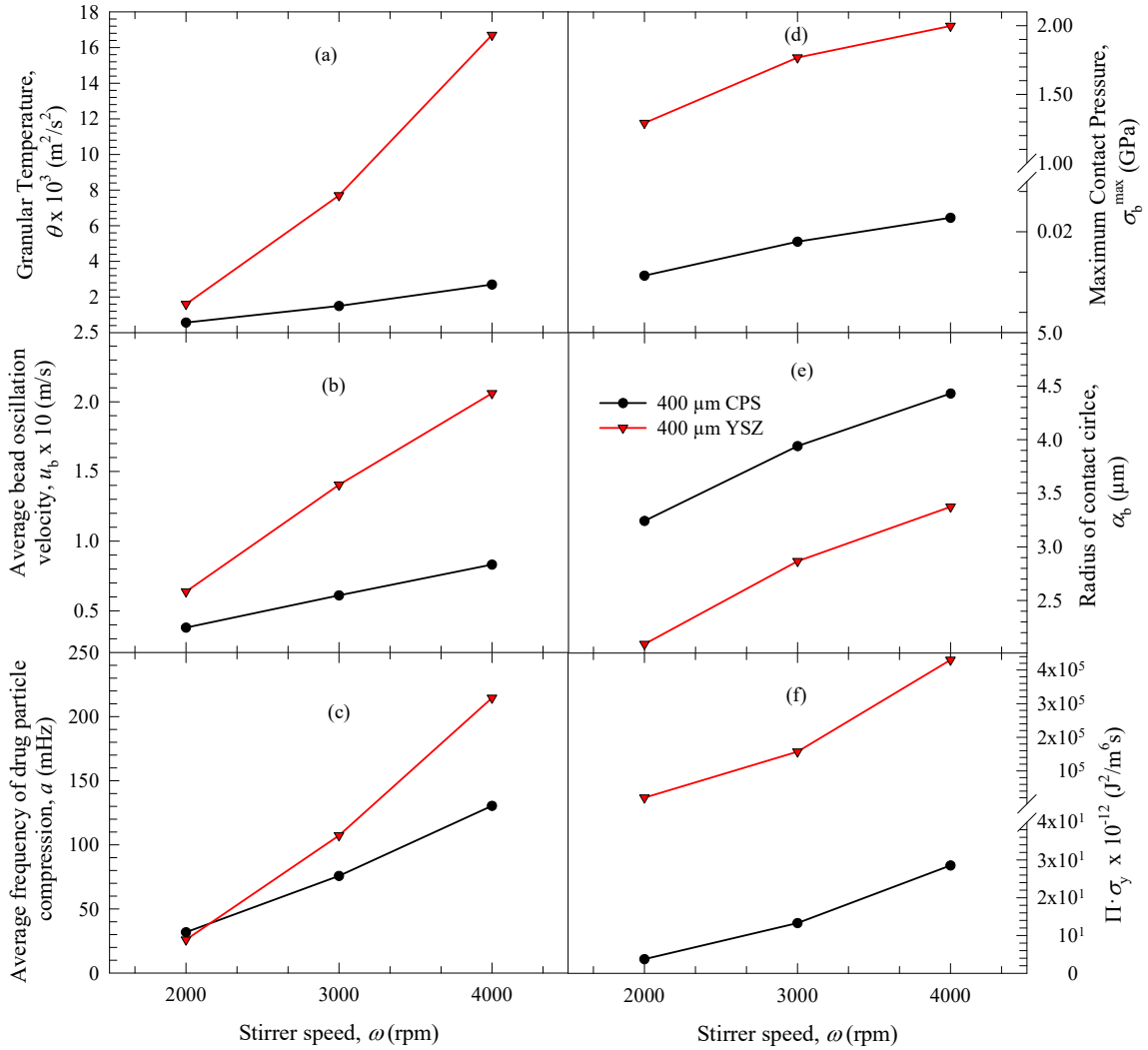


Figure 4.14 Effects of stirrer speed on (a) granular temperature θ , (b) the average bead oscillation velocity u_b , (c) the average frequency of drug particle compressions a , (d) the maximum contact pressure σ_b^{\max} , (e) radius of the contact circle α_b , and (f) the pseudo energy dissipation rate $\Pi \cdot \sigma_y$ when CPS and YSZ beads were used.

While the microhydrodynamics have revealed significant insights into the breakage kinetics when different process parameters and bead material were used, there is not a single microhydrodynamic parameter that can perfectly correlate to the observed breakage kinetics (Li et al., 2017). Moreover, while YSZ beads achieved much higher values of the

microhydrodynamic parameters than the CPS beads (except for α_b) especially at the higher speeds (Figure 4.14), which should lead to drastic increases in the breakage rate, the differences of the characteristic time constants for the two materials tended to converge at the higher speeds (Figure 4.13). This could be partly explained by the non-linear, complex relationships between the microhydrodynamic parameters and the breakage kinetics. More importantly, as explained in detail in Section 4.2.2, the breakage rate appears to be affected more by the average frequency of drug particle compressions a than the maximum contact pressure σ_b^{\max} provided that σ_b^{\max} is not too low, which may be the case at 2000 rpm. Also, the observation that despite exhibiting much higher σ_b^{\max} and $\Pi \cdot \sigma_y$ especially upon an increase in the stirrer speed (Figure 4.14d and 4.14f), the YSZ beads did not yield proportionally lower characteristic time constants; in fact, the time constants got closer at the higher speeds (Figure 4.13). This observation further supports the fatigue failure mechanism discussed in Section 4.2.2 in which the frequency of drug particle compressions a is the dominant factor as compared to σ_b^{\max} and $\Pi \cdot \sigma_y$ provided σ_b^{\max} is above a threshold value.

4.4. An Engineering Rationale for the Selection of Bead Material

The results in Section 3.3 overall suggest that YSZ beads can achieve a desired product fineness, which is dependent on the specific applications of drug nanoparticles, in a shorter duration than CPS beads (refer to Figure 4.13). This advantage of YSZ beads operationally translates into shorter cycle/production times (also lower costs) or production of more batches per manufacturing campaign. However, also illustrated in Figure 13, due to their higher density, YSZ beads required higher specific energy consumption than the CPS

beads, which adds to the operational cost. Hence, the choice of bead material from a manufacturing perspective depends on actual energy costs and labor costs that would be incurred as well as consideration of the speed needed to supply the market needs, which is beyond the scope of this manuscript. On the other hand, we defined a simple merit score by Eq. (4.3) considering both the cycle time–specific energy consumption. Figure 13 demonstrates that YSZ beads has a higher merit score than CPS beads considering both aspects. Even though the specific energy required was lower for the CPS beads (except $\omega = 2000$), the faster breakage associated with YSZ beads rendered them more favorable over CPS beads, as represented by the merit score.

The above discussion suggests that YSZ beads are more favorable from a manufacturing perspective considering only the cycle/production time–specific energy consumption within the experimental space examined. Based on the profiles in Figure 4.13, it is speculated that CPS beads may perform similar to the YSZ beads in terms of breakage kinetics/cycle time, and in fact may even be much more efficient considering that CPS beads require much less specific energy to break drug particles than the YSZ beads. However, due to the design limitation of our mill (4200 rpm), such extremely high speeds could not be evaluated in this study. Also, this study did not compare the YSZ and CPS beads in terms of media wear and contamination under different operating conditions. Although the contamination introduced by typical ceramic and polymeric milling beads is mostly not regulated by health authorities, they must be quantified in the lower ppm range, according to the current regulatory concepts and permitted daily exposures for oral, parenteral, pulmonary, and topical administration, as stated by Juhnke et al. (2012). Contamination must be quantified for a specific mill, media, and drug to be milled, as part

of a pharmaceutical development program. Juhnke et al. (2012) found contamination with 100–500 $\mu\text{g/g}$ Zr from three different grades of 100 μm YSZ beads when an undisclosed drug was wet-milled to 140 nm particles (unspecified time and batch size). Li et al. (2015) found that Zr contamination was similar order of magnitude in their study, but the contamination was reduced dramatically when 50 μm beads were used as opposed to 800 μm beads. Unfortunately, there is no published information about contamination with CPS beads during WSMM; the toxicological assessment of polystyrene, particularly leachables, is still under discussion.

CHAPTER 5

CONCLUSIONS AND OUTLOOK

CPS beads could be used effectively to prepare griseofulvin nanosuspensions with a median size < 200 nm within 256 min in wet stirred media milling. An increase in the stirrer speed led to faster breakage due to occurrence of more frequent bead–bead collisions with higher stress intensity. The CPS bead loading had two counteracting effects; at the higher bead loading, more frequent drug particle compressions a occurred albeit with lower maximum contact pressure σ_b^{\max} . The dominant effect associated with a on the faster breakage kinetics as compared with σ_b^{\max} emerges from a damage mechanism called contact fatigue for the drug particles when they are captured multiple times by the colliding beads. We provided a first microhydrodynamic verification of the commonly held notion that softer beads (CPS) should allow for a larger contact circle than harder beads (YSZ), which is advantageous to capturing fine drug particles during the milling. However, despite this advantage of the CPS beads, due to their lower fluctuating kinetic energy and oscillation velocity, they achieved a lower frequency of drug particle compressions a than the YSZ beads. The YSZ beads led to faster breakage than the CPS beads, but this came at a cost of higher power consumption and higher specific energy consumption due to the higher density of the YSZ beads. The consideration of both cycle/production time and specific energy consumption through a simple metric score suggests that YSZ beads outperformed the CPS beads from an engineering viewpoint for the specific experimental design space investigated here.

It is projected based on existing experimental trends that the CPS beads could perform similar to YSZ beads at stirrer speeds higher than 4000 rpm (> 14.7 m/s tip speed) in terms of breakage kinetics, with smaller specific energy consumption, which should be examined in a future study. Also, in order to generalize the findings in this study, future studies will use other BCS Class II drugs. Media wear and contamination aspects should be considered in a rigorous selection of the bead material.

The microhydrodynamic model suggests new processing modalities and new material designs of beads for enhancing milling efficiency, i.e., producing a desired fineness of drug particles fastest with the minimal specific energy consumption. One such approach is to use composite beads whose core consists of dense materials such as stainless steel that is covered by a coating of a wear-resistant polymer such as CPS, polyamide, polyurethane, etc. In fact, such composite beads are available commercially. Another approach could be designing new wear-resistant polymers with high density. Most commercially available wear-resistant, polymeric beads have densities lower than 2.0 g/cm^3 . Besides new bead design, a new processing modality may use a mixture of wear-resistant beads: hard/dense beads like YSZ and soft/light beads like CPS.

Finally, to better understand the dependence stirrer power on the process parameters such as stirrer speed and beads loading as well as geometry of the mill/beads, dimensionless correlations that relate power number to Reynolds (Re) number and Froude (Fr) number should be developed while taking into account the non-Newtonian nature of the drug nanosuspensions. Moreover, more research should be directed to developing a fundamental understanding of the different rheology exhibited by the suspensions prepared by CPS beads (pseudoplastic) vs. YSZ beads (Newtonian).

APPENDIX A

The dissipation coefficient R_{diss} is given by Wylie et al. (2003) as:

$$R_{\text{diss}} = R_{\text{diss0}}(c) + K(c)d_b\rho_L\theta^{1/2} / \mu_L \quad (\text{A.1})$$

where ρ_L is the density of the equivalent liquid and K is a coefficient given by the empirical correlation relating to the bead concentration given by:

$$K(c) = (0.096 + 0.142c^{0.212}) / (1-c)^{4.454} \quad (\text{A.2})$$

and R_{diss0} is the dissipation coefficient taking into account squeezing of the equivalent liquid film when two beads are approaching in the absence of liquid motion and is expressed as:

$$R_{\text{diss0}} = k_1(c) - k_2(c) \ln \varepsilon_m \quad (\text{A.3})$$

where ε_m is the nondimensional bead-bead gap thickness at which the lubrication force continually stops increasing and becomes constant. According to Sangani et al. (1996), ε_m can be taken at 0.003. k_1 and k_2 are calculated as follows:

$$k_1(c) = 1 + 3\sqrt{c/2} + (135/64)c \ln c + 11.26c(1 - 5.1c + 16.57c^2 - 21.77c^3) \quad (\text{A.4})$$

$$k_2(c) = c(1 - 0.5c) / (1-c)^3 \quad (\text{A.5})$$

Eq. (A.2)-(A.5) were used to calculate R_{diss} which is used in Eq. 3 of the main text to determine the granular temperature θ . With θ determined, all other microhydrodynamic parameters could then be determined as mentioned in the main text and also below. The average maximum normal force F_b^n is determined as follows:

$$F_b^n = 1.96 \left[\frac{Y_b}{(1-\eta_b^2)} \right]^{2/5} \rho_b^{3/5} R_b^2 \theta^{3/5} \quad (\text{A.6})$$

where Y_b and η_b are the Young modulus and Poisson's ratio of the bead. For CPS the values were taken as 1.5 GPa and 0.33, (He et al., 2008) respectively, and for YSZ these values were taken as 200 GPa and 0.2, (Ashby and Cebon, 1993; Srikar et al., 2004), respectively. R_b is the radius of bead and was taken as half the median size d_{50} . Next, the probability of a particle being caught between two colliding beads p is calculated with radius R_p is as follows:

$$p = 0.97 \frac{c}{1-c} \left[\frac{\rho_b (1-\eta_b^2)}{Y_b} \right]^{2/5} \theta^{2/5} \frac{R_p}{R_b} \quad (\text{A.7})$$

APPENDIX B

Table B.1 The Time it Takes for the Drug Median Size d_{50} to Reach $0.5 \mu\text{m}$ (t_{d50}) and d_{90} to Reach $1 \mu\text{m}$ (t_{d90}) and Characteristic Time Constant (τ_p) Fitted by the Empirical Model (Eq. (4.1)) to the Evolution of the Median Particle Size.

Run no.	Stirrer speed ω (rpm)	Bead Loading c (-)	Bead Material	Characteristic Milling Times ^a		Parameters of the Empirical Model Fit		
				t_{d50} (min)	t_{d90} (min)	d_{lim} (μm)	τ_p (min)	R^2
1	2000	0.198	CPS	(-) ^b	(-) ^b	0.175	112	0.933
2	2000	0.298	CPS	172	231	0.318	30.9	0.989
3	2000	0.397	CPS	52.4	106	0.176	12.5	0.935
4	2000	0.594	CPS	7.92	15.6	0.141	4.06	0.974
5	3000	0.198	CPS	156	240	0.301	24.2	0.986
6	3000	0.298	CPS	43.4	72.2	0.180	6.78	0.991
7	3000	0.397	CPS	17.4	31.8	0.168	4.79	0.992
8	3000	0.594	CPS	3.52	6.38	0.138	1.52	0.963
9	4000	0.198	CPS	50.2	77.4	0.175	7.93	0.990
10	4000	0.298	CPS	17.1	28.7	0.169	3.13	0.989
11	4000	0.397	CPS	8.22	15.5	0.149	2.11	0.977
12	4000	0.594	CPS	1.21	5.59	0.122	1.16	0.960
13	2000	0.594	YSZ	4.13	12.1	0.144	2.48	0.991
14	3000	0.594	YSZ	1.97	3.90	0.128	1.37	0.954
15	4000	0.594	YSZ	0.61	3.14	0.128	0.717	0.966

^aCalculated by Hermite interpolation.

^b d_{50} and d_{90} did not reach $0.5 \mu\text{m}$ and $1 \mu\text{m}$, respectively.

Table B.2 Values for Characteristic Milling Times (t_{d50} and t_{d90}), Energy Consumption for t_{d50} (E_{td50}), Energy Consumption for t_{d90} (E_{td90}), and Merit Scores for Run 2–15.

Run no. ^a	t_{d50} (min)	t_{d90} (min)	E_{td50} (J/g)	E_{td90} (J/g)	Merit score (–)
2	172	231	7040	9450	0.83
3	52.4	106	3240	6560	5.89
4	7.92	15.6	601	1190	210
5	156	240	10800	16500	0.60
6	43.4	72.9	3450	5800	6.68
7	17.4	31.7	1570	2850	36.7
8	3.52	6.38	540	977	527
9	50.1	77.4	5930	9140	3.36
10	17.1	28.7	2560	4300	22.8
11	8.22	14.5	1490	2630	81.6
12	1.21	5.59	305	1410	2710
13	4.13	12.1	570	1600	407
14	1.97	3.90	759	1500	669
15	0.61	3.14	473	2450	3480

^aRun 1 was not considered as d_{50} and d_{90} did not reach 0.5 μm and 1 μm , respectively.

Table B.3 Power Applied Per Unit Volume P_w , Apparent Shear Viscosity μ_L and Density ρ_L of the Milled Drug Suspensions Measured, and Dynamic Viscosity μ_m and Mixture Density ρ_m of the Slurries Estimated for Runs 1–15.

Run no.	P_w (W/m ³)	μ_L (mPa·s)	ρ_L (kg/m ³)	μ_m (mPa·s) ^a	ρ_m (kg/m ³) ^b
1	8.20×10 ⁴	140	1030	278	1030
2	1.70×10 ⁵	138	1030	465	1030
3	2.58×10 ⁵	132	1020	1180	1030
4	3.16×10 ⁵	99.3	1030	2.78×10 ⁴	1040
5	2.87×10 ⁵	143	1030	284	1030
6	3.31×10 ⁵	117	1030	394	1030
7	3.75×10 ⁵	112	1040	997	1040
8	6.39×10 ⁵	73.0	1030	2.05×10 ⁴	1040
9	4.92×10 ⁵	141	1030	280	1030
10	6.25×10 ⁵	126	1030	425	1030
11	7.56×10 ⁵	107	1030	953	1030
12	1.05×10 ⁶	62.5	1030	1.75×10 ⁴	1040
13	5.51×10 ⁵	49.4	1060	1.38×10 ⁴	3990
14	1.61×10 ⁶	18.1	1020	5.07×10 ³	3980
15	3.25×10 ⁶	8.31	1030	2.33×10 ³	3980

^a $\mu_m = \mu_L[1 + 2.5c + 10c^2 + 0.0019\exp(20c)]$ from Gillies and Shook (2000)

^b $\rho_m = \rho_b c + \rho_L(1-c)$

Table B.4 Power applied per unit volume P_w and all microhydrodynamic parameters (θ , u_b , ν , σ_b^{\max} , α_b , a , and $\Pi \cdot \sigma_y$) calculated for Runs 1–15.

Run no.	P_w (W/m ³)	θ (m ² /s ²)	u_b (m/s)	ν (KHz)	σ_b^{\max} (GPa)	α_b (μ m)	a (mHz)	$\Pi \cdot \sigma_y$ (J ² /m ⁶ s)
1	8.20×10^4	2.40×10^{-3}	7.89×10^{-2}	0.52	2.09×10^{-2}	4.33	0.79	0.456×10^{12}
2	1.70×10^5	2.10×10^{-3}	7.39×10^{-2}	1.04	2.03×10^{-2}	4.21	3.58	1.22×10^{12}
3	2.58×10^5	1.60×10^{-3}	6.39×10^{-2}	1.77	1.93×10^{-2}	3.99	8.49	2.25×10^{12}
4	3.16×10^5	5.66×10^{-4}	3.80×10^{-2}	4.52	1.56×10^{-2}	3.24	31.9	3.75×10^{12}
5	2.87×10^5	8.20×10^{-3}	1.45×10^{-1}	0.96	2.67×10^{-2}	5.53	3.34	2.25×10^{12}
6	3.31×10^5	4.80×10^{-3}	1.11×10^{-1}	1.55	2.40×10^{-2}	4.97	7.47	3.57×10^{12}
7	3.75×10^5	2.70×10^{-3}	8.28×10^{-2}	2.29	2.14×10^{-2}	4.43	13.6	4.43×10^{12}
8	6.39×10^5	1.50×10^{-3}	6.11×10^{-2}	7.28	1.90×10^{-2}	3.94	75.7	13.3×10^{12}
9	4.92×10^5	1.41×10^{-2}	1.90×10^{-1}	1.26	2.98×10^{-2}	6.17	5.42	4.55×10^{12}
10	6.25×10^5	8.40×10^{-3}	1.46×10^{-1}	2.05	2.68×10^{-2}	5.56	12.3	7.38×10^{12}
11	7.56×10^5	5.60×10^{-3}	1.12×10^{-1}	3.30	2.47×10^{-2}	5.13	26.2	11.4×10^{12}
12	1.05×10^6	2.70×10^{-3}	8.32×10^{-2}	9.90	2.14×10^{-2}	4.43	130	28.5×10^{12}
13	5.51×10^5	1.60×10^{-3}	6.38×10^{-2}	8.04	1.29	2.09	26.0	2.04×10^{16}
14	1.61×10^6	7.70×10^{-3}	1.40×10^{-1}	17.7	1.77	2.87	107	1.57×10^{17}
15	3.25×10^6	1.67×10^{-2}	2.06×10^{-1}	26.0	2.00	3.37	215	4.30×10^{17}

The apparent shear viscosities of the milled suspensions and an aqueous stock solution of the stabilizers were measured using an R/S plus Brookfield Rheometer (Brookfield Engineering, Middleboro, MA, USA) at $25\text{ }^{\circ}\text{C} \pm 0.5\text{ }^{\circ}\text{C}$ with a coaxial cylinder (CC40). Samples from the suspensions were sheared at a shear rate from 0 to 1000 1/s over a period of 60 s and μ_L was taken at the maximum shear rate in accordance with earlier studies (Berhnhart, et al, 1999). Fig. S1 illustrates several general patterns: (i) all suspensions prepared with the CPS beads exhibited pseudoplasticity, whereas those prepared with YSZ beads exhibited near-Newtonian behavior and had lower apparent shear viscosity at the same bead loading; (ii) an increase in the CPS beads loading or an increase in the stirred speed led to lower viscosity. The latter observation could be mainly explained by a decrease in d_{50} of the milled suspensions at higher bead loading–stirrer speed as GF nanosuspensions with finer particles are known to have lower viscosity (Li et al., 2017). The pseudoplastic behavior may have originated from the presence of soft aggregates or clusters of drug nanoparticles–polymer/SDS, which were broken as the shear rate was increased during the viscosity testing, leading to a decrease of apparent viscosity. Higher extent of aggregate/cluster breakage (deaggregation) upon an increase in the shear rate is well-known (refs.). The aggregates/clusters in a nanosuspension can occlude liquid in their void space, which increases the effective volume fraction of the solid in a suspension with fixed solids loading. Hence, in general, an aggregated suspension has a higher shear viscosity than a fully dispersed suspension consisting of discrete primary particles. Since the GF aggregates broke more extensively at the higher shear rates, the apparent shear viscosity decreased with an increase in shear rate during the viscosity testing of the suspensions

prepared with the CPS beads. It is speculated that under the highly energetic milling conditions (Runs 13–15) associated with the YSZ beads, which are signified by the highest P_w , σ_b^{\max} , and $\Pi \cdot \sigma_y$ among all runs with the same beads loading (see Table S4), these clusters were permanently (irreversibly) destroyed during the milling, which explains the near-Newtonian behavior and lower apparent viscosity at the higher stirrer speeds. Since the milling conditions with the CPS beads were much less energetic than those with the YSZ beads, it is likely that these clusters either survived in the milling process or broken clusters were reversibly reformed prior to the viscosity testing. Unfortunately, due to the invasive nature of the particle sizing via laser diffraction (dilution), such clusters in the suspensions prepared with the CPS beads vs. the dispersed particles in the suspensions prepared with the YSZ beads was not clearly differentiated by laser diffraction measurements.

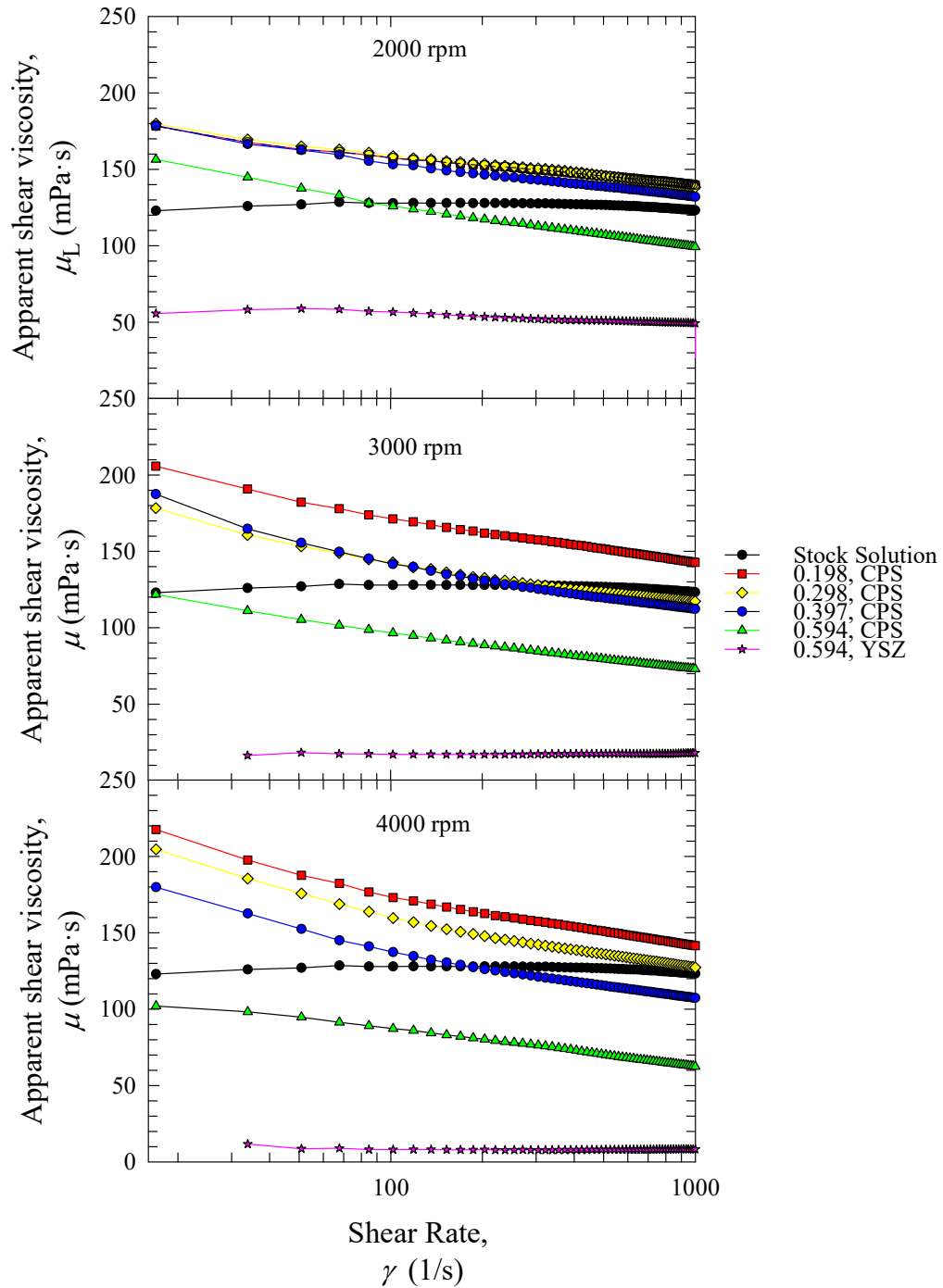


Figure B.1 Apparent shear viscosity of the milled suspensions prepared in Runs 1–15 at various stirrer speeds: (a) $\omega = 2000$ rpm, (b) $\omega = 3000$ rpm, and (c) $\omega = 4000$ rpm, along with that of the aqueous stock solution of the stabilizers (5% HPC SL grade and 0.5% SDS), shown for baseline comparison. The stock solution was not processed in the mill.

APPENDIX C

Symbols

a	average frequency of drug particle compressions, Hz
c	fractional volumetric concentration of the beads, –
d	particle or bead diameter, m
E_{td50}	specific energy consumption during t_{d50} (J/g)
E_{td90}	specific energy consumption during t_{d90} (J/g)
F_b^n	average maximum normal force during collision of two identical elastic beads, N
k	restitution coefficient for bead–bead collisions, –
K	coefficient obtained from an empirical correlation, –
m	mass (g)
p	probability for a single drug particle to be caught between the beads, –
P	power applied by the mill stirrer (rotor), W
P_w	average power consumption per unit volume (stirrer power), W/m ³
Q	volumetric flow rate of the drug suspension, m ³ /s
R	radius, m
R_{diss}	dissipation (effective drag) coefficient of the bead, –
R_{diss0}	dissipation coefficient when relative motion of the bead–liquid is absent, –
t	milling time, s
t_{d50}	milling time required to attain a median drug particle size d_{50} of 0.5 μm , s
t_{d90}	milling time required to attain a 90% passing size d_{90} of 1 μm , s

u_b	average bead oscillation velocity, m/s
V_m	volume of the milling chamber, m ³
Y	Young modulus, Pa
Y^*	reduced elastic modulus for the bead–drug contact, Pa

Greek letters

α_b	radius of the contact circle formed at the contact of two beads, m
ε	volumetric fraction of drug particles in the drug suspension, –
ε_{coll}	energy dissipation rate due to partially inelastic bead–bead collisions, W/m ³
ε_{ht}	power spent on shear of equivalent liquid of the slurry at the same shear rate but calculated (measured) as if no beads were present in the flow, W/m ³
ε_m	non-dimensional bead–bead gap thickness at which the lubrication force stops increasing and becomes a constant, –
ε_{tot}	total energy dissipation rate, W/m ³
ε_{visc}	energy dissipation rate due to both the liquid–beads viscous friction and lubrication, W/m ³
η	Poisson’s ratio, –
μ_L	apparent shear viscosity of the equivalent fluid, Pa·s
ν	frequency of single-bead oscillations, Hz
Π	energy dissipation rate attributed to the deformation of drug particles per unit volume, W/m ³
$\Pi \cdot \sigma_y$	pseudo energy dissipation rate, J ² /m ⁶ s
θ	granular temperature, m ² /s ²

ρ	density, kg/m ³
σ_b^{\max}	maximum bead contact pressure at the center of the contact circle, Pa
σ_y	contact pressure in a drug particle when the fully plastic condition is obtained, Pa
τ_p	characteristic time constant of the milling process, s
ω	stirrer (rotational) speed, rpm

Indices

b	bead
D	total drug
L	equivalent liquid (milled drug suspension)
p	drug particle
y	yield
50	50% passing size (median size) of the cumulative distribution
90	90% passing size of the cumulative distribution

REFERENCES

- Afolabi, A., Akinlabi, O., Bilgili, E., 2014. Impact of process parameters on the breakage kinetics of poorly water-soluble drugs during wet stirred media milling: A microhydrodynamic view. *Eur. J. Pharm. Sci.* 51, 75–86.
- Annapragada, A.; Adjei, A. Numerical simulation of milling processes as an aid to process design. *Int. J. Pharm.* 1996, 136, 1–11
- Ashby, M.F., Cebon, D., 1993. Materials selection in mechanical design. *Le Journal de Physique IV* 3, C7-1–C7-9.
- Barthelmes, G., Pratsinis, S., Buggisch, H., 2003. Particle size distributions and viscosity of suspensions undergoing shear-induced coagulation and fragmentation. *Chem Eng Sci.* 58 (13), 2893–902.
- Basa, S., Muniyappan, T., Karatgi, P., Prabhu, R., Pillai, R., 2008. Production and in vitro characterization of solid dosage form incorporating drug nanoparticles. *Drug Dev. Ind. Pharm.* 34, 1209–1218.
- Bernhardt, C., Reinsch, E., Husemann, K., 1999. The influence of suspension properties on ultra-fine grinding in stirred ball mills. *Powder Technol.* 105, 357–361.
- Bhakay, A., Merwade, M., Bilgili, E., Dave, R.N., 2011. Novel aspects of wet milling for the production of microsuspensions and nanosuspensions of poorly water-soluble drugs. *Drug Dev. Ind. Pharm.* 37, 963–976.
- Bhakay, A., Rahman, M., Davé, R.N., Bilgili, E., 2018 Bioavailability Enhancement of Poorly-Water Soluble Drugs via Nanocomposites: Formulation–Processing Aspects and Challenges. *Pharmaceutics*. Vol. 10, Issue 3, 86.
- Bhakay, A., Vizzotti, E., Li, M., Davé R., Bilgili, E., 2016. Incorporation of fenofibrate nanoparticles prepared by melt emulsification into polymeric films. *J. Pharm. Innov.* 11, 53–63.
- Bilgili, E., Afolabi, A., 2012. A combined microhydrodynamics–polymer adsorption analysis for elucidation of the roles of stabilizers in wet stirred media milling. *Int. J. Pharm.* 439, 193–206.
- Bilgili, E., Hamey, R., Scarlett, B., 2006. Nano-milling of pigment agglomerates using a wet stirred media mill: Elucidation of the kinetics and breakage mechanisms. *Chem. Eng. Sci.* 61, 149-157.

- Bilgili, E., Li, M., Afolabi, A., 2016. Is the combination of cellulosic polymers and anionic surfactants a good strategy for ensuring physical stability of BCS Class II drug nanosuspensions? *Pharm. Dev. Technol.* 21, 499–510.
- Bitterlich, A., Laabs, C., Krautstrunk, I., Dengler, M., Juhnke, M., Grandeury, A., Bunjes, H., Kwade, A., 2015. Process parameters dependent growth phenomena of naproxen nanosuspension manufactured by wet media milling. *Eur. J. Pharm. Biopharm.* 92, 171–179.
- Cao, J., Cheng, Z., Fang, Y., Jing, H., Huang, J., Wang, Y., 2008. Simulation and experimental studies on fluidization properties in a pressurized jetting fluidized bed. *Powder Technol.* 183, 127–132.
- Cerdeira, A.M., Mazzotti, M., Gander, B., 2010. Miconazole nanosuspensions: influence of formulation variables on particle size reduction and physical stability. *Int. J. Pharm.* 396, 210–218.
- Cerdeira, A.M., Mazzotti, M., Gander, B., 2011. Role of milling parameters and particle stabilization on nanogrinding of drug substances of similar mechanical properties. *Chem. Eng. Tech.* 34, 1427–1438.
- Cooper, E.R. Nanoparticles: A personal experience for formulating poorly water-soluble drugs. *J. Control. Release* 2010, 141, 300–302.
- Dai, W.G., Dong, L.C., Song, Y.Q., 2007. Nanosizing of a drug/carrageenan complex to increase solubility and dissolution rate. *Int. J. Pharm.* 342, 201–207.
- Date, A.A.; Patravale, V. Current strategies for engineering drug nanoparticles. *Curr. Opin. Colloid Interface Sci.* 2004, 9, 222–235.
- Deng, Z., Xu, S., Li, S., 2008. Understanding a relaxation behavior in a nanoparticle suspension for drug delivery applications. *Int. J. Pharm.* 351, 236–243.
- Eskin, D., Zhupanska, O., Hamey, R., Moudgil, B., Scarlett, B., 2005a. Microhydrodynamic analysis of nanogrinding in stirred media mills. *AIChE J.* 51, 1346–1358.
- Eskin, D., Zhupanska, O., Hamey, R., Moudgil, B., Scarlett, B., 2005b. Microhydrodynamics of stirred media milling. *Powder Technol.* 156, 95–102.
- Fakes, M.G., Vakkalagadda, B.J., Qian, F., Desikan, S., Gandhi, R.B., Lai, C., Hsieh, A., Franchini, M.K., Toale, H., Brown, J., 2009. Enhancement of oral bioavailability of an HIV-attachment inhibitor by nanosizing and amorphous formulation approaches. *Int. J. Pharm.* 370, 167–174.

- Feng, T., Pinal, R., Carvajal, M.T., (2008). Process induced disorder in crystalline materials: differentiating defective crystals from the amorphous form of griseofulvin. *J. Pharm. Sci.* 97, 3207–3221.
- Forrest, W.P., Reuter, K.G., Shah, V., Kazakevich, I., Heslinga, M., Dudhat, S., Patel, S., Neri, C., Mao, Y., 2018. USP Apparatus 4: A valuable in vitro tool to enable formulation development of long-acting parenteral (LAP) nanosuspension formulations of poorly water-soluble compounds. *Am. Assoc. Pharm. Sci.* 19, 413–424.
- Ghosh, I., Schenck, D., Bose, S., Ruegger, C., 2012. Optimization of formulation and process parameters for the production of nanosuspension by wet media milling technique: Effect of Vitamin E TPGS and nanocrystal particle size on oral absorption. *Eur. J. Pharm. Sci.* 47, 718–728.
- Gidaspow, D., 1994. *Multiphase Flow and Fluidization: Continuum and Kinetic Theory Descriptions*. Academic Press. Cambridge, Massachusetts.
- Gillies, G.G., Shook, C.A., 2000. Modelling high concentration settling slurry flows. *Can. J. Chem. Eng.* 78, 709–716.
- He, J.Y., Zhang, Z.L., Midttun, M., Fonnum, G., Modahl, G.I., Kristiansen, H., Redford, K., 2008. Size effect on mechanical properties of micron-sized PS-DVB polymer particles. *Polymer.* 49, 3993–3999.
- Ito, A., Konnerth, C., Schmidt, J., Peukert, W., 2016. Effect of polymer species and concentration on the production of mefenamic acid nanoparticles by media milling. *Eur. J. Pharm. Biopharm.* 98, 98–107.
- Juhnke, M., Berghausen, J., Timpe, C., 2010. Accelerated formulation development for nanomilled active pharmaceutical ingredients using a screening approach. *Chem. Eng. Technol.* 33, 1412–1418.
- Juhnke, M., Martin, D., John, E., 2012. Generation of wear during the production of drug nanosuspensions by wet media milling. *Eur. J. Pharm. Biopharm.* 81, 214–222.
- Kawatra, S.K., 2006. *Advances in Comminution*. Society for Mining Metallurgy, Englewood, Colorado.
- Kakran, M., Sahoo, N.G., 2012. Preparation of nanoparticles of poorly water-soluble antioxidant curcumin by antisolvent precipitation methods. *J. Nanopart. Res.* 14(757)
- Kim, J.H., Jang, S.W., Han, S.D., Hwang, H.D., Choi, H.-G., 2011. Development of a novel pphthamic ciclosporin A-loaded nanosuspension using top-down media milling methods. *Pharmazie.* 66, 491–495.

- Knieke, C., Azad, M., Davé, R., Bilgili, E., 2013. A study of the physical stability of wet media-milled fenofibrate suspensions using dynamic equilibrium curves. *Chem. Eng. Res. Des.* 91, 1245–1258.
- Knieke, C., Sommer, M., Peukert, W., 2009. Identifying the apparent and true grinding limit. *Powder Technol.* 195, 25–30.
- Koradia, K.D., Sheth, N.R., Koradia, H.D., Dabhi, M.R., 2018. Ziprasidone nanocrystals by wet media milling followed by spray drying and lyophilization: formulation and process parameter optimization. *J. Drug. Del. Sci. and Tech.* 43, 73–84.
- Kumar, S., Burgess, D.J., 2014. Wet milling induced physical and chemical instabilities of naproxen nano-crystalline suspensions. *Int. J. Pharm.* 466, 223–232.
- Kwade, A. Wet comminution in stirred media mills—Research and its practical application. *Powder Technol.* 1999, 105, 14–20.
- Kawatra, S.K. *Advances in Comminution*; Society for Mining, Metallurgy and Exploration: Englewood, CO, USA, 2006.
- Leung, D., Lamberto, D., Liu, Lina., Kwong, E., Nelson, T., Rhodes, T., Bak, A., 2014. A new and improved method for the preparation of drug nanosuspension formulations using acoustic mixing technology. *Int. J. Pharm.* 473, 10–19.
- Li, M., Alvarez, P., Bilgili, E., 2017. A microhydrodynamic rationale for selection of bead size in preparation of drug nanosuspensions via wet stirred media milling. *Int. J. Pharm.* 524, 178–192.
- Li, M., Azad, M., Davé, R., Bilgili, E., 2016a. Nanomilling of drugs for bioavailability enhancement: A holistic formulation–process perspective. *Pharmaceutics* 8, 17.
- Li, M., Lopez, N., Bilgili, E., 2016b. A study of the impact of polymer–surfactant in drug nanoparticle coated pharmatose composites on dissolution performance. *Adv. Powder Technol.* 27, 1625–1636.
- Li, M., Yaragudi, N., Afolabi, A., Davé, R., Bilgili, E., 2015. Sub-100 nm drug particle suspensions prepared via wet milling with low bead contamination through novel process intensification. *Chem. Eng. Sci.* 130, 207–220.
- Malamatari, M., Taylor, K.M.G., Malamtaris, S., Douroumis, D., Kachrimanis, K., 2018. Pharmaceutical nanocrystals: production by wet milling and applications. *Drug Discov. Today.* 23, 534–547.
- Mannheim, V., 2011. Empirical and scale-up modeling in stirred ball mills. *Chem. Eng. Res. Des.* 89, 405–409.

- Merisko-Liversidge, E., Liversidge, G.G., 2011. Nanosizing for oral and parenteral drug delivery: A perspective on formulating poorly-water soluble compounds using wet media milling technology. *Adv. Drug Deliver. Rev.* 63, 427–440.
- Merisko-Liversidge, E., Liversidge, G.G., Cooper, E.R., 2003. Nanosizing: a formulation approach for poorly-water-soluble compounds. *Eur. J. Pharm. Sci.* 18, 113–120.
- Müller, R.H., Jacobs, C., Kayser, O., 2001. Nanosuspensions as particulate drug formulations in therapy rationale for development and what we can expect for the future. *Adv. Drug. Deliv. Rev.* 47, 3–19.
- Muller, R.H., Keck, C.M., 2004. Challenges and solutions for the delivery of biotech drugs – a review of drug nanocrystal technology and lipid nanoparticles. *J. Biotechnol.* 113, 151–170.
- Nakach, M., Authelin, J.-R., Agut, C., 2017. New approach and practical modelling of bead milling process for the manufacturing of nanocrystalline suspensions. *J. Pharm. Sci.* 106, 1889–1904.
- Nakach, M., Authelin, J.-R., Perrin, M.-A., Lakkireddy, H.R., 2018. Comparison of high pressure homogenization and stirred bead milling for the production of nanocrystalline suspensions. *Int. J. Pharm.* 547, 61–71.
- Nakach, M., Authelin, J.-R., Tadros, T., Galet, L., Chamayou, A., 2014. Engineering of nano-crystalline drug suspensions: Employing a physico-chemical based stabilizer selection methodology or approach. *Int. J. Pharm.* 476, 277–288.
- Noyes, A.A., Whitney, W.R., 1897. The rate of solution of solid substances in their own solutions. *J. Am. Chem. Soc.* 19, 930–934.
- Onoue, S., Kawabata, Y., Seto, Y., Hatanaka, J., Timmermann, B., Yamada, S., 2009. Formulation design and photochemical studies on nanocrystal solid dispersion of curcumin with improved oral bioavailability. *J. Pharm. Sci.* 99, 1871–1881.
- Patel, D.J.; Patel, J.K.; Pandya, V.M. Improvement in the dissolution of poorly water soluble drug using media milling technique. *Thai J. Pharm. Sci.* 2010, 34, 155–164.
- Peltonen, L., Hirvonen, J., 2010. Pharmaceutical nanocrystals by nanomilling: critical process parameters, particle fracturing, and stabilization methods. *J. Pharm. Pharmacology.* 62, 1569–1579.
- Quinn, K., Gullapalli, R.P., Merisko-Liversidge, E., Goldbach, E., Wong, A., Liversidge, G.G., Hoffman, W., Sauer, J.-M., Bullock, J., Tonn, G., 2012. A Formulation strategy for gamma secretase inhibitor ELND006, a BCS class II compound:

- Development of a nanosuspension formulation with improved oral bioavailability and reduced food effects in dogs. *J. Pharm. Sci.* 101, 1462–1474.
- Rundfeldt, C., Steckel, H., Scherliess, H., Wyska, E., Wlaź, Piotr., 2013. Inhalable highly concentrated itraconazole nanosuspension for the treatment of bronchopulmonary aspergillosis. *Eur. J. Pharm. Biopharm.* 83, 44–53.
- Sangani, A.S., Mo, G., Tsao, H.-K., Koch, D.L., 1996. Simple shear flows of dense gas-solid suspensions at finite Stokes numbers. *J. Fluid Mech.* 313, 309–341.
- Silva, A.C., Gonzales-Mira, E., Garcia, M.A., Egea, M.A., Silva, R., Santos, D., Souto, E.B., Ferreira, D., 2011. Preparation, characterization and biocompatibility studies of risperidone-loaded solid lipid nanoparticles (SLN): high pressure homogenization versus ultrasound. *Col. Surf. B: Biointer.* 86, 158–165.
- Singh, S.K.; Srinivasan, K.; Gowthamarajan, K.; Singare, D.S.; Prakash, D.; Gaikwad, N.B. Investigation of preparation parameters of nanosuspension by top-down media milling to improve the dissolution of poorly water-soluble glyburide. *Eur. J. Pharm. Biopharm.* 2011, 78, 441–446.
- Srikar, V., Turner, K.T., Andrew Ie, T.Y., Spearing, S.M., 2004. Structural design considerations for micromachined solid-oxide fuel cells. *J. Power Sources* 125, 62–69.
- Stražičar, J., Runovc, F., 1996. Kinetics of comminution in micro- and sub-micrometer ranges. *Int. J. Miner. Process.* 44, 673–682.
- Sun, W., Mao, S., Shi, Y., Chiu, L., Fang, L., 2011. Nanonization of itraconazole by high pressure homogenization: stabilizer optimization and effect of particle size on oral absorption. *J. Pharm. Sci.* 100, 3365–3373.
- Tanaka, Y.; Inkyo, M.; Yumoto, R.; Nagai, J.; Takano, M.; Nagata, S. Nanoparticulation of probucol, a poorly water-soluble drug, using a novel wet-milling process to improve *in vitro* dissolution and *in vivo* oral absorption. *Drug Dev. Ind. Pharm.* 2012, 38, 1015–1023.
- Tatsumi, S., Murayama, Y., Hayakawa, H., Sano, M., 2009. Experimental study on the kinetics of granular gases under microgravity. *J. Fluid Mech.* 641, 521–539.
- Thombre, A.-M., Shah, J.-C., Sagawa, K., Caldwell, B.-W., 2012. *In vitro* and *in vivo* characterization of amorphous, nanocrystalline, and crystalline ziprasidone formulations. *Int. J. Pharm.* 428, 8–17.
- Toziopoulou, F., Malamataris, M., Nikolakakis, I., Kachrimanis, K., 2017. Production of aprepitant nanocrystals by wet media milling and subsequent solidification. *Int. J. Pharm.* 533, 324–334.

- Van Eerdenbrugh, B., Van den Mooter, G., Augustijns, P., 2008. Top-down production of drug nanocrystals: nanosuspension stabilization, miniaturization and transformation into solid products. *Int. J. Pharm.* 364, 64–75.
- Van Eerdenbrugh, B., Vermant, J., Martens, J.A., Froyen, L., Humbeeck, J.V., Augustijns, P., Van den Mooter, G., 2009. A screening study of surface stabilization during the production of drug nanocrystals. *J. Pharm. Sci.* 98, 2091–2103.
- Varinot, C., Berthiaux, H., Dodds, J., 1999. Prediction of the product size distribution in associations of stirred bead mills. *Powder Technol.* 105, 228–236.
- Wylie, J.J., Koch, D.L., Ladd, A.J., 2003. Rheology of suspensions with high particle inertia and moderate fluid inertia. *J. Fluid Mech.* 480, 95–118.
- Yadav, D., Kumar, N., 2014. Nanonization of curcumin by antisolvent precipitation; process development, characterization, freeze drying and stability performance. *Int. J. Pharm.* 477, 564–577.
- Ye, Y., Zhang, X., Zhang, T., Wang, H., Wu, B., 2014. Design and evaluation of injectable niclosamide nanocrystals prepared by wet media milling technique. *Drug Dev. Ind. Pharm.*